The Astronomical Journal, 155:91 (17pp), 2018 February https://doi.org/10.3847/1538-3881/aaa45b

Searching for Be Stars in the Open Clusters with PTF/iPTF. I. Cluster Sample and Be Star Candidates

Po-Chieh Yu (俞伯傑)[1], Chang-Hsien Yu (游昌憲)[1], Chien-De Lee (李建德)[1], Chien-Cheng Lin (林建爭)[2,3], Chih-Hao Hsia (夏志浩)[4], Chang-Kao Chang (章展誥)[1], I-Chenn Chen (陳以忱)[1], Chow-Choong Ngeow (饒兆聰)[1], Wing-Huen Ip (葉永烜)[1,4,5], Wen-Ping Chen (陳文屏)[1,6], Russ Laher (良主嶺亞)[7], Jason Surace[8], and Shrinivas R. Kulkarni[9]

[1] Graduate Institute of Astronomy, National Central University, No. 300, Zhongda Road, Zhongli Dist., Taoyuan City 32001, Taiwan
[2] Key Laboratory for Research in Galaxies and Cosmology, Shanghai Astronomical Observatory, Chinese Academy of Sciences, 80 Nandan Road, Shanghai 200030, People's Republic of China
[3] Max Planck Institute for Astronomy, Königstuhl 17, D-69117 Heidelberg, Germany
[4] Space Science Institute, Macau University of Science and Technology, Avenida Wai Long, Taipa, Macau
[5] Institute of Space Science, National Central University, No. 300, Zhongda Road, Zhongli Dist., Taoyuan City 32001, Taiwan
[6] Department of Physics, National Central University, No. 300, Zhongda Road, Zhongli Dist., Taoyuan City 32001, Taiwan
[7] Infrared Processing and Analysis Center, California Institute of Technology, Pasadena, CA 91125, USA
[8] Spitzer Science Center, California Institute of Technology, M/S 314-6, Pasadena, CA 91125, USA
[9] Division of Physics, Mathematics and Astronomy, California Institute of Technology, Pasadena, CA 91125, USA
Received 2017 June 6; revised 2017 December 26; accepted 2017 December 26; published 2018 January 29

Abstract

We conducted a search for Be star candidates in open clusters using Hα imaging photometry of the Palomar Transient Factory Survey to investigate some connections among Be star phenomena, cluster environments, and ages. Stellar members of clusters were identified by spatial distributions, near-infrared magnitudes and colors, and by proper motions. Among 104 open clusters, we identified 96 Be star candidates in 32 clusters; 11 of our candidates have been reported in previous studies. We found that the clusters with age $7.5 < \log(t(\mathrm{year})) \leqslant 8.5$ tend to have more Be star candidates; there is about a 40% occurrence rate within this age bin. The clusters in this age bin also tend to have a higher Be fraction N(Be)/N(Be+B-type). These results suggest that the environments of young and intermediate clusters are favorable to the formation of Be phenomena. Spatial distribution of Be star candidates with different ages implies that they do not form preferentially in the central regions. Furthermore, we showed that the mid-infrared (MIR) colors of the Be star candidates are similar to known Be stars, which could be caused by free–free emission or bound-free emission. Some Be star candidates might have no circumstellar dust according to their MIR colors. Finally, among 96 Be candidates, we discovered that one Be star candidate FSR 0904-1 exhibits long-term variability on the timescale of ∼2000 days with an amplitude of 0.2–0.3 mag, indicating a long timescale of disk evolution.

Key words: open clusters and associations: general – stars: emission-line, Be – stars: general – surveys

1. Introduction

Non-supergiant B-type stars with hydrogen emission lines, historically Hβ or more intense Hα emission lines, are called Be stars (Merrill et al. 1925; Jaschek et al. 1981). It is commonly accepted that their Balmer emission lines originated from circumstellar disks. The formation of the disks might be due to joined effects of fast rotation and of non-radial pulsations or magnetic fields (Lee et al. 1991; Porter & Rivinius 2003; Carciofi et al. 2009). By means of fast rotation with 70%–80% of the break-up velocity (Townsend et al. 2004), material of the stellar surface can be removed to form the circumstellar disk. Using near-infrared spectro-interferometry with high spectral resolution ($\lambda/\Delta\lambda \sim 12{,}000$), Kraus et al. (2012) studied the kinematics of two Be stars, β Canis Minoris and ζ Tauri, and concluded that the disk is in Keplerian rotation. Their results also support the decretion disk model, e.g., the disk is replenished by the material from the star (Rivinius et al. 2013; Klement et al. 2015). Some Be stars exhibit photometric and spectroscopic variability that could be caused by stellar winds or pulsations (Rivinius et al. 2003; McSwain et al. 2009; Barnsley & Steele 2013; Rivinius et al. 2016; Chojnowski et al. 2017; Labadie-Bartz et al. 2017; Pápics et al. 2017). Moreover, Be stars are also characterized by infrared color excess, which might be due to free–free and bound-free radiation from the ionized gas of the disks (Woolf et al. 1970; Allen 1973; Dachs & Wamsteker 1982; Lee & Chen 2011; Chen et al. 2016; Lee et al. 2016).

It is a mystery why only some B-type stars are Be stars. To answer this question, the essential step is to reveal the origin/formation of the fast rotator. The first possibility is that they are natural fast rotators. Some B-types stars have been found to have a rapid rotator with an equatorial velocity of ∼200 km s^{-1} (McNally 1965; Saio et al. 2017). Another hypothesis is that Be stars could be the consequence of binary interactions. Mass gainer stars might be spun-up to fast rotators through the transfer of mass and angular momentum (McSwain & Gies 2005). Another explanation is that they could become fast rotators during the main sequence evolution (Fabregat & Torrejón 2000), or near the turn-off (Keller et al. 2001). These Be stars are found in young (∼10 Myr) star clusters in the Milky Way (MW) galaxy (Mathew et al. 2008), Large Magellanic Cloud, and Small Magellanic Cloud (SMC; Wisniewski & Bjorkman 2006).

Collecting a large sample of Be stars is crucial to understanding their nature. Recently, several large spectroscopic and photometric surveys have been conducted to search

for Be stars. Using the INT Photometric Hα Survey of the Northern Galactic Plane (IPHAS; Drew et al. 2005), Raddi et al. (2015) spectroscopically confirmed 247 faint Be stars with brightness $13 < r < 16$ mag in the direction of the Perseus Arm. Chojnowski et al. (2015) presented 128 new Be stars with high-resolution near-infrared spectra ($\lambda/\Delta\lambda = 22{,}500$) from the Apache Point Observatory Galactic Evolution Experiment (APOGEE; Majewski et al. 2015). Also, Lin et al. (2015) discovered 180 Be stars identified by the Large Sky Area Multi-Object fiber Spectroscopic Telescope (LAMOST; Cui et al. 2012).

Because age information of Be stars is the key to studying their evolutions, it is necessary to collect Be stars in a sample of star clusters, as members of clusters share similar ages and environments. The enhancement of Be stars in young clusters has been found in several surveys (McSwain & Gies 2005; Wisniewski & Bjorkman 2006; Mathew et al. 2008; Mathew & Subramaniam 2011; Marsh Boyer et al. 2012; Tarasov & Malchenko 2012). McSwain & Gies (2005) conducted an extensive survey of Be stars in 55 open clusters of the MW. They showed an increase of Be fraction with age until 100 Myr, and concluded that Be stars should be spun-up during binary interactions. Mathew et al. (2008) conducted a Be star survey with slitless spectroscopy in 207 open clusters and found that only about 20% of the clusters have Be stars. Using optical spectroscopy, Mathew & Subramaniam (2011) investigated Be stars in 39 open clusters and found that 48% of their Be stars have Hα equivalent width (EW) in the range from −10 to −30 Å. They also discovered that spectra of more than 80% of Be stars show Fe II lines. Furthermore, Martayan et al. (2009) searched for Be stars in 84 open clusters of the SMC; they showed that Be stars in the SMC are 2–4 times more abundant than in the MW. This effect is likely caused by lower metallicity of the SMC (see detailed review in Rivinius et al. 2013).

Modern surveys with wide field cameras, such as the Palomar Transient Factory (PTF; Law et al. 2009) and intermediate PTF[10] (iPTF; Kulkarni 2013), benefit not only from time saving in a comprehensive survey, but also the coverage of an entire cluster occupying a wide sky area. The data of PTF/iPTF were taken by the 48 inch Samuel Oschin Telescope located at Palomar Observatory, using an 11-CCD-mosaic camera with a 7.3 square-degree field of view. The PTF/iPTF project employed various camera filters (some have yet to be documented), including broadband filters for the *g*, *R*, and *i* bands, and narrow-band filters for Hα 6563 Å (on), and Hα 6630 Å (off), and, more recently, for Hα 6720 Å and Hα 6810 Å. The wide field of the PTF/iPTF Hα images allow us to conduct a program to search for Be star candidates in open clusters of different ages (Yu et al. 2015, 2016). In the first of a series (Paper I), we present the cluster sample and their basic properties in Section 2. In Section 3, we describe the data and the method of identifying cluster membership and Be star candidates. We present our results and discussions in Section 4 and summarize this study in Section 5. In Paper II, we will investigate the spectroscopic properties of the Be star candidates. In Paper III, optical variability of a large Be star sample will be presented using current archival light curves and the incoming Zwicky Transient Facility survey[11] (ZTF; Kulkarni 2016).

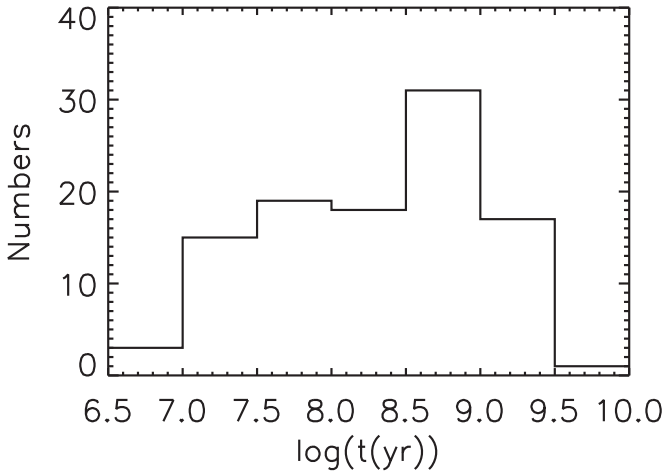

Figure 1. Age distribution of the cluster sample. Our sample covers cluster ages from a few Myr to a few Gyr.

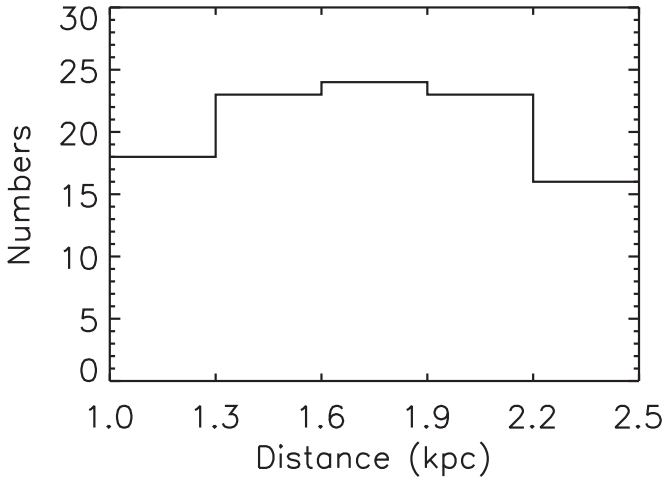

Figure 2. Distance distribution of the cluster sample. Our sample covers clusters with distance from the Sun between 1 and 2.5 kpc.

2. Cluster Sample

We selected 104 clusters from Kharchenko et al. (2013) on the basis of following criteria: (1) to study the connection between Be star and ages, we have selected cluster ages with $6.5 < \log(t(\text{year})) \leqslant 10$ (Figure 1); (2) to avoid difficulties of membership identification near the Galactic center, we have selected clusters located at Galactic-longitude range $30° < l < 240°$; (3) to avoid too many bright, and to extend the sample of faint, Be stars, we constrained cluster distance from the Sun within $1\,\text{kpc} < D < 2.5\,\text{kpc}$ (Figure 2). Table 1 lists the properties of the cluster sample. Notes about individual clusters are listed in Appendix. In this study, we only present clusters with more detailed studies in the Appendix.

[10] https://www.ptf.caltech.edu/iptf

[11] https://www.ptf.caltech.edu/ztf

Table 1
Basic Properties of the Cluster Sample

Name	R.A. (hh:mm:ss.ss)	Decl. (dd:mm:ss.ss)	$\mu_\alpha \cos\delta$ (mas yr^{-1})	μ_δ (mas yr^{-1})	Distance (kpc)	log (t (year))	Uncert. (years)	Size (arcmin)	N(Be)/ K(Be)	N(Be +B-type)	References
Mayer 1	00:22:03.36	61:44:27.60	−3.87	−3.27	1.430	7.74	⋯	9.8	0	23	⋯
Stock 20	00:25:15.36	62:36: 7.20	−2.56	−3.24	1.100	8.34	⋯	12.5	1	25	⋯
Stock 21	00:30:14.64	57:55:51.60	−1.07	−2.76	1.700	8.82	⋯	4.1	3	9	⋯
NGC 381	01:08:25.92	61:34:44.40	0.22	−2.07	1.200	8.85	0.029	9.7	0	21	⋯
Stock 3	01:12:09.12	62:15:28.80	−0.13	−0.64	1.363	7.85	⋯	2.6	0	3	⋯
ASCC 6	01:47:16.80	57:40:48.00	−0.52	−0.68	1.350	7.80	⋯	13.1	0	26	⋯
NGC 744	01:58:34.80	55:28:40.80	−0.30	−3.92	1.382	8.38	⋯	17.4	3	49	⋯
NGC 743	01:58:37.20	60:09:25.20	−1.81	−2.77	1.100	8.29	0.090	55.8	4	275	⋯
ASCC 7	01:59:06.00	58:55:30.00	1.94	−1.21	2.000	7.40	⋯	24.9	0	161	⋯
Czernik 6	02:01:55.20	62:51:00.00	−3.85	0.05	1.391	7.98	⋯	3.9	0	3	⋯
Stock 5	02:04:32.64	64:21:18.00	1.12	−1.16	1.100	7.70	⋯	5.0	0	8	⋯
NGC 869	02:18:57.60	57:08:42.00	−2.81	0.05	2.300	7.28	⋯	20.7	14/15	498	(d)
Basel 10	02:19:29.52	58:18:14.40	−0.75	1.62	2.000	7.60	⋯	8.7	1	16	⋯
NGC 884	02:22:02.88	57:08:42.00	−4.00	1.65	2.345	7.20	⋯	13.9	12–13	253	(d)
NGC 886	02:23:26.88	63:45:18.00	−1.47	0.52	1.000	8.75	⋯	24.4	1	43	⋯
Czernik 8	02:33:01.20	58:46:04.80	−0.60	−0.26	1.410	8.18	⋯	6.3	0	6	⋯
NGC 957	02:33:30.48	57:34:22.80	−1.01	1.39	1.900	7.25	⋯	10.0	1/2,4	48	(e), (f)
Czernik 12	02:39:22.32	54:54:46.80	−0.78	−0.34	2.000	9.10	⋯	3.0	0	4	⋯
SAI 24	02:59:27.60	60:32:60.00	−1.42	−0.20	1.000	7.20	⋯	9.7	0	17	⋯
NGC 1220	03:11:41.28	53:20:49.20	0.30	0.40	2.100	8.20	⋯	3.0	0/1	3	(j)
King 5	03:14:46.32	52:41:49.20	0.60	0.40	2.200	9.09	0.020	6.5	2	10	⋯
Czernik 15	03:23:12.00	52:13:58.80	1.42	−0.01	2.500	7.30	⋯	4.0	0	9	⋯
NGC 1348	03:34:12.00	51:23:60.00	1.92	−3.35	1.800	8.45	⋯	6.5	0	11	⋯
Tombaugh 5	03:48:03.60	59:04:12.00	1.20	−1.42	1.350	8.85	0.014	15.5	0	47	⋯
FSR 0663	04:06:10.80	51:54:36.00	−3.33	2.00	1.700	8.91	0.078	6.5	0	4	⋯
NGC 1502	04:07:49.92	62:19:51.60	0.01	−0.54	1.023	7.08	⋯	17.0	0	36	⋯
NGC 1513	04:09:42.00	49:30:36.00	−1.08	−3.49	1.400	8.50	⋯	15.0	3	43	⋯
Berkeley 11	04:20:27.60	44:54:54.00	−1.73	−6.53	1.964	8.70	⋯	5.4	1	10	⋯
FSR 0728	04:29:52.80	38:30:00.00	−2.04	−7.40	1.816	8.26	0.100	8.0	0	8	⋯
Berkeley 67	04:37:48.00	50:46:30.00	0.09	−1.49	2.000	9.24	0.029	10.4	0	5	⋯
FSR 0714	04:42:46.80	41:55:01.20	−1.42	−0.20	1.819	9.06	⋯	5.6	0	1	⋯
Berkeley 68	04:44:27.60	42:06:00.00	−5.86	0.30	1.800	9.11	⋯	4.3	0	0	⋯
FSR 0717	04:46:08.40	42:07:48.00	−3.13	−1.48	1.700	9.05	⋯	8.3	0	4	⋯
NGC 1664	04:51:13.92	43:39:36.00	−4.23	−4.20	1.200	8.75	0.023	13.9	1	39	⋯
NGC 1778	05:07:58.80	37:01:40.80	−0.76	−7.59	1.500	8.45	⋯	9.2	1/3	28	(g)
IRAS 05100 +3723	05:13:27.12	37:26:16.80	−4.24	−7.07	2.238	7.40	⋯	5.2	0	9	⋯
Czernik 20	05:20:27.60	39:32:24.00	−3.76	−1.12	2.000	9.19	0.048	3.3	0	1	⋯
Berkeley 17	05:20:37.20	30:35:24.00	3.90	−2.31	1.800	9.60	⋯	9.6	0	0	⋯
SAI 47	05:23:56.40	42:19:22.80	−2.81	−2.58	1.523	9.20	⋯	6.5	0	0	⋯
FSR 0777	05:27:36.96	34:44:52.80	1.40	−4.27	1.173	7.00	⋯	4.8	0	11	⋯
NGC 1907	05:28:04.80	35:19:30.00	0.85	−5.70	1.600	8.60	⋯	7.9	0	37	⋯
Stock 8	05:28:08.40	34:25:26.40	1.16	−5.36	1.731	7.05	⋯	7.5	0	30	⋯
FSR 0736	05:29:07.44	44:46:12.00	−1.44	−4.75	1.800	9.34	0.057	6.4	0	0	⋯
FSR 0749	05:32:06.72	41:37:04.80	3.19	1.13	2.300	8.62	0.071	8.7	2	8	⋯
NGC 1960	05:36:19.68	34:09:28.80	0.91	−4.35	1.200	7.57	0.078	15.5	0/5	60	(h)
Koposov 36	05:36:47.76	31:11:60.00	2.94	−8.86	1.600	8.45	0.021	6.3	0	4	⋯
FSR 0816	05:39:19.68	31:30:57.60	1.40	−8.85	2.220	7.80	⋯	8.8	1	7	⋯
Koposov 27	05:39:33.12	33:21:28.80	2.75	−3.62	2.500	8.76	0.052	4.2	0	2	⋯
FSR 0799	05:42:16.08	33:39:36.00	0.08	−3.74	2.473	9.10	⋯	14.1	1	34	⋯
FSR 0826	05:42:52.80	28:57:25.20	2.19	−2.18	2.100	7.30	⋯	7.6	0	7	⋯
FSR 0850	05:45:07.20	24:44:16.80	0.07	−3.88	1.836	7.30	⋯	15.8	0	42	⋯
Koposov 10	05:47:30.00	35:25:08.40	4.47	−4.56	1.819	8.78	⋯	4.2	0	3	⋯
Czernik 23	05:50:06.00	28:53:60.00	−2.11	−2.32	2.449	8.48	⋯	3.6	0	6	⋯
FSR 0852	05:53:29.28	25:10:22.80	3.16	−0.97	2.149	9.00	⋯	7.5	0	6	⋯
Koposov 12	06:01:02.64	35:16:37.20	0.92	−1.80	1.900	8.91	⋯	9.3	0	23	⋯
NGC 2129	06:01:06.24	23:20:24.00	1.89	−1.43	1.651	7.48	⋯	8.5	0/2	20	(b), (c)
IC 2157	06:04:49.68	24:04:12.00	−0.54	−3.01	2.311	7.90	⋯	4.5	0	16	⋯
FSR 0833	06:05:24.00	30:47:34.80	−0.43	−4.15	2.088	9.10	0.029	6.5	0	0	⋯
FSR 0942	06:05:58.80	13:39:36.00	−0.98	−1.77	2.082	9.00	⋯	4.1	0	3	⋯
FSR 0904	06:07:03.12	19:01:19.20	1.63	−6.72	1.427	7.80	⋯	7.0	1	12	⋯

Table 1
(Continued)

Name	R.A. (hh:mm:ss.ss)	Decl. (dd:mm:ss.ss)	$\mu_\alpha \cos\delta$ (mas yr^{-1})	μ_δ (mas yr^{-1})	Distance (kpc)	log (t (year))	Uncert. (years)	Size (arcmin)	N(Be)/ K(Be)	N(Be +B-type)	References
FSR 0858	06:09:10.08	25:40:48.00	0.52	−1.48	2.127	9.01	0.057	3.9	0	2	⋯
NGC 2175	06:09:41.28	20:30:18.00	1.92	−7.55	1.636	7.00	⋯	57.1	0/1	515	(a)
FSR 0952	06:10:17.28	13:01:01.20	−1.16	−1.84	1.994	9.11	0.025	18.4	0	16	⋯
Pismis 27	06:10:55.20	20:36:54.00	0.98	−4.03	1.664	8.25	0.203	4.0	0	9	⋯
FSR 0939	06:10:58.08	14:23:45.60	0.16	1.54	2.397	8.71	⋯	8.5	0	12	⋯
FSR 0968	06:11:21.84	11:52:15.60	−0.40	−1.80	2.187	8.52	0.045	8.1	0	27	⋯
FSR 0956	06:12:25.20	13:01:12.00	−1.50	−0.26	2.180	8.10	⋯	5.3	0	4	⋯
FSR 0940	06:14:14.88	14:48:00.00	−0.11	1.25	2.421	9.40	⋯	5.7	0	8	⋯
Kronberger 12	06:14:14.88	22:28:58.80	−1.04	−5.85	1.893	8.87	0.084	4.0	1	2	⋯
BDSB 82	06:14:59.28	12:20:16.80	0.17	0.07	1.934	7.92	0.151	4.7	0	4	⋯
FSR 0891	06:17:34.08	22:25:37.20	−0.46	−5.32	2.075	8.37	⋯	3.0	0	5	⋯
FSR 0902	06:18:18.00	20:32:24.00	−0.51	−5.50	1.243	7.14	⋯	11.9	1	21	⋯
FSR 0953	06:19:02.16	14:07:48.00	−0.21	2.92	1.734	8.75	0.082	4.3	0	1	⋯
Skiff J0619 +18.5	06:19:21.84	18:30:36.00	−0.78	−3.00	1.380	7.90	⋯	19.3	8	50	⋯
FSR 0951	06:22:20.16	14:42:18.00	−0.26	−0.84	1.619	8.70	⋯	6.6	0	21	⋯
Dolidze 22	06:23:14.16	04:35:24.00	−1.14	−1.42	1.775	8.37	⋯	5.3	1	6	⋯
FSR 0955	06:23:50.88	14:30:54.00	0.90	0.02	1.994	7.40	⋯	4.3	2	7	⋯
FSR 1033	06:28:20.88	02:56:06.00	0.59	−3.52	1.710	8.52	⋯	6.5	0	3	⋯
Juchert 18	06:31:27.12	06:48:14.40	−1.81	−2.04	2.290	9.02	0.040	3.4	0	2	⋯
NGC 2244	06:31:55.20	04:56:24.00	−0.84	−0.94	1.532	6.70	⋯	16.2	1	59	⋯
FSR 0974	06:32:34.80	12:32:34.80	1.05	−1.16	2.308	8.91	0.031	3.6	0	4	⋯
FSR 0905	06:33:42.48	22:17:16.80	0.35	−4.59	1.786	8.30	0.064	5.8	3	10	⋯
Basel 8	06:34:12.00	08:00:36.00	−2.04	−0.47	1.432	7.92	0.099	27.0	3	103	⋯
Collinder 107	06:38:30.24	04:38:06.00	−2.50	−0.26	1.447	7.17	0.016	3.6	0	5	⋯
Collinder 110	06:38:42.00	02:02:06.00	2.28	−2.55	2.362	9.22	0.010	19.8	7	47	⋯
NGC 2269	06:43:12.00	04:36:54.00	−0.50	−2.00	1.585	8.66	⋯	7.2	0	15	⋯
Alessi 16	06:43:33.60	02:10:30.00	−0.98	−2.14	2.088	8.65	⋯	4.4	0	11	⋯
FSR 1025	06:50:28.80	06:35:60.00	−1.65	−1.70	2.095	8.60	⋯	3.9	0	3	⋯
FSR 1029	06:54:02.40	06:43:30.00	0.78	−3.98	1.905	8.93	⋯	6.1	0	5	⋯
FSR 0866	06:55:14.40	29:43:48.00	−1.19	−1.00	1.664	9.20	⋯	8.2	0	2	⋯
FSR 1147	08:00:19.20	01:15:36.00	−3.30	2.93	1.508	8.72	0.016	14.9	0	7	⋯
NGC 6811	19:37:22.08	46:23:42.00	−5.68	−6.70	1.227	8.80	0.017	3.6	0	9	⋯
NGC 6866	20:03:56.88	44:09:36.00	−2.75	−4.80	1.326	8.64	0.027	12.7	4	31	⋯
Dolidze 1	20:09:42.48	36:29:52.80	−1.59	0.09	1.445	7.60	⋯	6.4	0	0	⋯
NGC 6910	20:23:15.12	40:47:42.00	−4.27	−5.72	1.127	7.53	0.026	40.1	1/1	45	(i)
FSR 0213	20:26:59.04	38:58:19.20	−2.59	−3.73	1.434	8.71	0.065	8.4	0	9	⋯
Patchick 103	20:34:55.92	53:17:45.60	−4.94	−5.20	1.332	8.95	⋯	6.3	0	0	⋯
CBJC 4	20:56:17.52	44:23:24.00	−6.78	−3.67	1.293	7.70	⋯	12.3	0	12	⋯
Collinder 428	21:03:04.32	44:33:36.00	−5.81	−1.78	1.185	8.86	⋯	6.4	0	3	⋯
FSR 0253	21:03:30.72	39:58:48.00	−3.72	−0.62	1.414	8.28	⋯	13.6	7	14	⋯
NGC 7031	21:07:06.00	50:52:30.00	−1.95	−4.01	1.100	8.20	⋯	49.1	0	95	⋯
FSR 0354	22:11:09.60	57:39:36.00	−2.80	−3.64	1.169	8.00	⋯	14.4	2	33	⋯
FSR 0398	22:36:14.40	64:07:58.80	−2.37	−0.45	1.200	7.70	⋯	20.9	0	23	⋯
NGC 7654	23:24:42.48	61:38:13.20	−0.23	−3.50	1.350	7.90	⋯	20.7	2	132	⋯

Note. Column 1: Names of clusters. Column 2: Right Ascension (R.A.) in hms (J2000). Column 3: Declination (decl.) in hms (J2000). Column 4: Proper motion of R.A. Column 5: Proper motion of decl. Column 6: Distance of clusters to the Sun. Column 7: Logarithm of the cluster age (t). Column 8: Uncertainties of ages in logarithm. Column 9: Size of searching region. Column 10: Numbers of Be star candidates of clusters found in this work (N(Be)). The notation K(Be) is known Be star numbers from literature. Column 11: Numbers of B-type stars in clusters. Column 12: References of known Be stars: (a) Zhang et al. (2008), (b) Morgan et al. (1955), (c) WEBDA: https://www.univie.ac.at/webda/; (d) Marsh Boyer et al. (2012), (e) Schild & Romanishin (1976), (f) Mathew et al. (2008), (g) Barbon & Hassan (1973), (h) Souza et al. (2016), (i) Kubát et al. (2007), (j) Mathew & Subramaniam (2011).

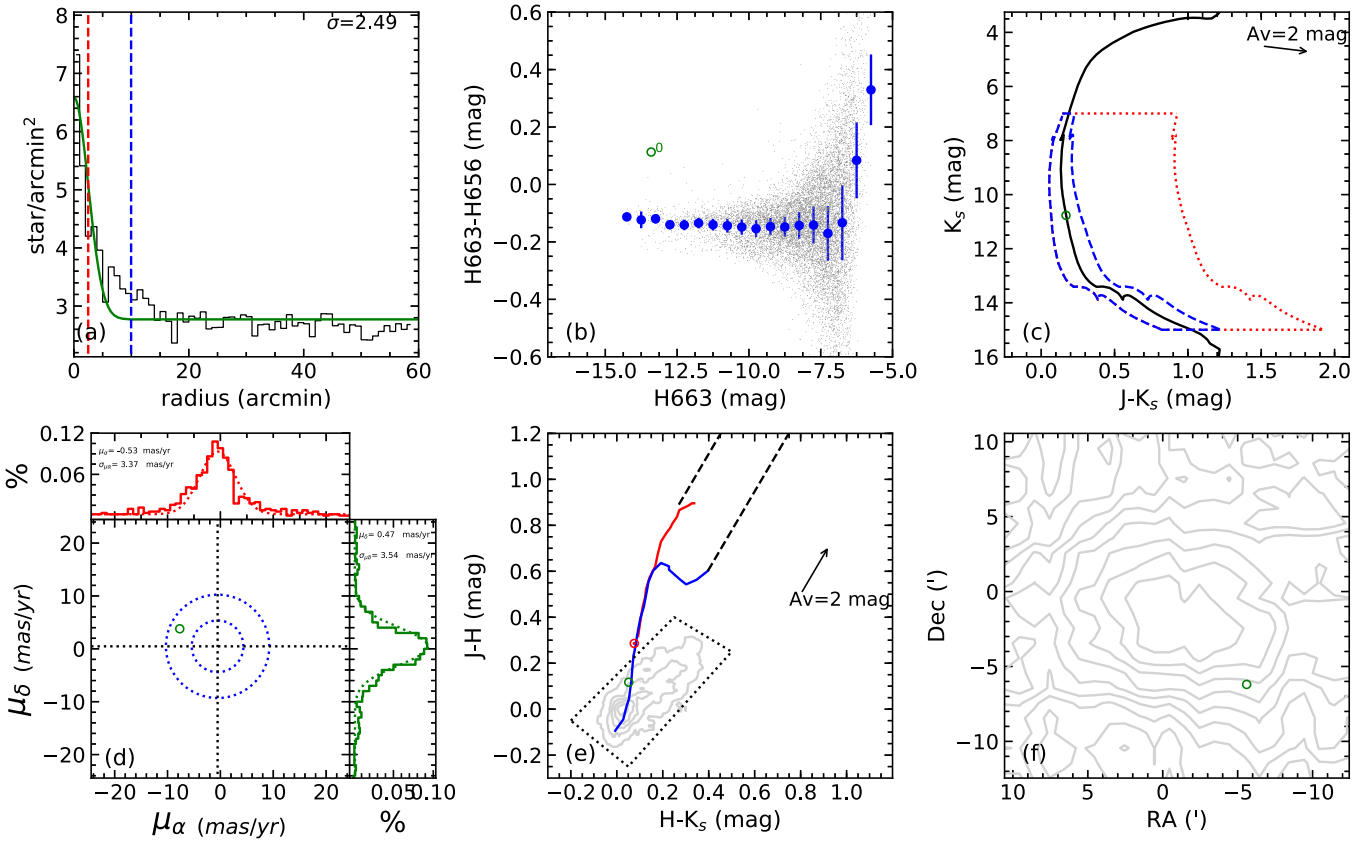

Figure 3. Example of identification of Be star candidates and membership of NGC 957. The green open circle represents the Be candidate in the cluster in panel (b)–(f). (a) Determination of cluster size by Gaussian fitting. The blue dashed line is the 4σ width, and the red dashed line is the 1σ width. (b) Selection of Hα emitters. Blue filled circles represent mean colors and their photometric scattering of Hα-on and -off filters. Gray dots represent stars within the survey region. Stars are selected as emission-line candidates if they have excess colors of HA663-HA656. (c) Membership identification using 2MASS CMD. The black line indicates the isochrone. While non-emission-line stars are considered to be members within the blue-dashed region, Be star candidates are regarded as photometric members within the red dashed region. (d) Membership identification using PMs. The inner and outer blue dashed circles represent $1\sigma_\mu$ and $2\sigma_\mu$ regions. Stars are considered as kinematic members if their PMs are within the $2\sigma_\mu$ regions. (e) Selection of Be candidates from Hα emitters using 2MASS color–color diagram. The gray contours show the known Be stars distributions. Hα emitters are selected as Be candidates within the dashed box. The red and blue curves show the giant and dwarf loci (Bessell & Brett 1988) converted to the 2MASS system. The arrow represents the reddening direction (Rieke & Lebofsky 1985) for typical Galactic interstellar extinction ($Rv = 3.1$), and the dashed lines encompass the region of reddened giants and dwarfs. (f) Spatial distribution of cluster and Be candidates.

3. Data Analysis and Method

3.1. Determination of the Searching Region

We used the radial density profile to determine the searching region (Figure 3(a)). We have selected stars from the PPMXL[12] (Roeser et al. 2010) data with a signal-to-noise ratio (S/N) $\geqslant$ 10 in the Two Micron All Sky Survey (2MASS; Cutri et al. 2003) J, H, and K_s bands. Because 10% of objects of PPNXL include spurious entries (Roeser et al. 2010), Kharchenko et al. (2012) have averaged and computed their PMs and errors. Here, we used these PMs instead of PPMXL data. Then we used the half-Gaussian fitting of the radial density profile to determine a 3σ radius. As some open clusters have irregular shapes due to their evolution processes, we adopted a box with the side of 8σ ($2 \times 4\sigma$) region as the searching region for these open clusters.

3.2. Searching for Emission-line Candidates

We used differential photometry with Hα-on and -off images from PTF/iPTF to identify Hα emission-line candidates (Figure 3(b)). The Hα-on and -off images were taken through HA656 and HA663 narrow-band filters (Law et al. 2009) and were processed for bias corrections, flat fielding, and astrometric calibration (Laher et al. 2014). As the Hα emitters can exhibit excess colors of HA663−HA656 (e.g., flux excess in HA656 image), we selected candidates that stand out in the HA663−HA656 colors. We adopted different selection criteria for stars with different brightness because faint stars have increased scattering of the HA663−HA656 colors due to photometric errors. We first calculated the photometric scattering (σ_p) of HA663−HA656 colors within each 0.5 mag bin of HA663. Then we selected probable Hα emitters for those with HA663−HA656 $> 2\sigma_p + \mathrm{mean_{color}}$, whereas $\mathrm{mean_{color}}$ is the mean of HA663−HA656 colors within each 0.5 mag bin of HA663. We only show the emission-line candidates after membership identification in Figure 3(b) (green open circle).

3.3. Identifying Photometric Membership

To characterize the membership of emission-line star candidates, we used near-infrared (NIR) photometric data of 2MASS that provides a 10σ detection limit in the J, H, and K_s bands. We defined a region of photometric membership by estimating $J - K_s$ errors propagated from photometric errors of

[12] http://vizier.u-strasbg.fr/viz-bin/VizieR?-source=%20PPMXL

Table 2
Basic Properties of Be Star Candidates

Object	R.A. (hh:mm:ss.ss)	Decl. (dd:mm:ss.ss)	$\mu_\alpha \cos\delta$ (mas yr^{-1})	μ_δ (mas yr^{-1})	$J-H$ (mag)	$H-K_s$ (mag)	R (mag)	SIMBAD
Stock 20-1	00:25:27.12	62:42:37.13	−3.0	0.1	0.037	0.109	11.400	⋯
Stock 21-3	00:30:06.16	57:56:01.97	−2.6	−1.5	0.171	0.067	13.160	⋯
Stock 21-2	00:30:09.54	57:56:33.12	−6.9	−1.8	0.116	0.113	13.370	⋯
Stock 21-1	00:30:23.97	57:56:30.29	−1.3	0.8	0.109	0.104	12.770	⋯
NGC 743-4	01:58:01.31	60:56:45.61	−6.3	3.3	0.263	0.174	13.070	⋯
NGC 744-13	01:58:11.73	55:42:18.68	0.2	6.8	0.208	0.092	11.230	⋯
NGC 743-3	01:58:21.22	59:53:59.89	−8.1	2.2	0.201	0.146	13.370	⋯
NGC 744-1	01:59:29.50	55:26:23.48	−0.5	−4.7	0.035	0.043	11.470	⋯
NGC 744-5	01:59:33.00	55:29:34.02	2.6	−8.8	0.152	0.065	12.680	⋯
NGC 743-1	02:00:10.06	60:10:53.49	1.6	−1.0	0.285	0.298	11.350	Be
NGC 743-2	02:00:31.68	59:53:58.97	5.8	3.2	0.120	0.049	11.950	⋯
NGC 869-2	02:16:47.63	57:17:38.52	1.6	3.0	0.158	0.089	12.210	⋯
NGC 869-1	02:17:30.82	57:17:47.30	2.0	−3.2	0.106	0.051	12.110	iC
NGC 869-4	02:18:18.73	57:22:01.75	−3.9	−5.4	0.227	0.164	14.240	iC
NGC 869-3	02:18:24.29	57:21:42.26	−6.3	−2.9	0.175	0.109	13.890	iC
NGC 869-16	02:19:05.87	57:13:57.39	−2.2	−6.9	0.152	0.114	12.220	iC
NGC 869-26*	02:19:08.63	57:03:48.99	−1.4	−0.9	0.289	0.215	12.420	Be (B5)
NGC 869-14	02:19:29.23	57:09:48.19	3.5	0.1	0.102	0.046	11.650	iC
NGC 869-17	02:19:33.22	57:15:08.42	−5.3	−3.8	0.095	0.077	12.370	iC
NGC 869-18	02:19:58.29	57:10:15.42	−6.7	3.3	0.185	0.140	13.670	iC
NGC 869-20	02:19:59.28	57:21:43.78	−1.2	−2.1	0.152	0.139	14.640	⋯
NGC 886-1	02:20:03.78	63:37:24.80	−3.2	3.0	0.344	0.273	13.400	Em
NGC 869-15	02:20:04.05	57:03:19.72	−5.0	2.9	0.106	0.050	11.760	iC
NGC 869-25	02:20:07.68	57:18:56.18	−0.6	10.3	0.177	0.129	13.210	iC
Basel 10-1	02:20:20.34	58:19:32.51	0.4	6.5	0.220	0.331	11.690	Be
NGC 884-2	02:20:57.89	57:18:27.55	−1.7	−2.6	0.122	0.055	11.390	iC
NGC 869-19	02:21:03.28	56:59:49.67	−7.0	−0.8	0.272	0.138	14.260	iC
NGC 884-14	02:21:03.28	56:59:49.67	−7.0	−0.8	0.272	0.138	14.260	iC
NGC 869-27*	02:21:24.91	57:11:52.57	−5.7	8.3	0.196	0.215	12.186	Be (B2)
NGC 884-19*	02:21:24.91	57:11:52.57	−5.7	8.3	0.196	0.215	12.190	Be (B2)
NGC 884-11	02:21:33.88	56:56:15.72	−4.4	−4.8	0.170	0.094	12.960	iC
NGC 884-6	02:21:46.02	57:11:26.42	−4.9	2.0	0.067	0.129	13.520	iC
NGC 884-1	02:21:46.43	57:14:07.81	3.1	−1.3	0.174	0.074	11.290	iC
NGC 884-12	02:21:47.92	57:15:21.27	−3.7	1.2	0.199	0.132	13.310	iC
NGC 884-8	02:22:10.08	57:03:02.85	−5.8	−8.1	0.090	0.036	12.260	iC
NGC 884-13	02:22:10.18	57:20:53.83	−4.8	−1.1	0.211	0.087	14.360	iC
NGC 884-4	02:22:23.04	57:03:48.56	−6.6	2.8	0.083	0.040	12.370	iC
NGC 884-3	02:23:07.12	57:04:54.54	−5.7	4.2	0.134	0.085	12.700	iC
NGC 884-5	02:23:19.90	57:17:20.91	−3.3	3.0	0.227	0.127	13.250	iC
NGC 957-1*	02:33:08.19	57:28:10.88	−7.7	3.8	0.117	0.052	11.650	Be
King 5-1	03:14:21.74	52:40:47.19	−0.4	1.3	0.194	0.151	13.540	⋯
King 5-3	03:15:19.71	52:38:00.72	−1.3	0.4	0.223	0.164	15.150	⋯
NGC 1513-3	04:09:43.44	49:28:42.55	−2.6	−2.7	0.290	0.177	13.450	iC
NGC 1513-1	04:10:08.22	49:26:54.55	−0.5	−6.1	0.142	0.132	12.330	iC
NGC 1513-2	04:10:17.53	49:27:49.96	−1.3	−8.9	0.166	0.071	12.820	iC
Berkeley 11-1	04:20:26.86	44:52:44.79	−6.5	−2.5	0.300	0.164	14.660	⋯
NGC 1664-1	04:52:08.05	43:42:07.39	−1.1	0.9	0.078	0.055	12.420	iC
NGC 1778-1*	05:08:11.74	36:57:02.85	3.5	−6.8	0.095	0.100	11.030	⋯
FSR 0749-2	05:31:41.67	41:33:35.36	−0.7	0.5	0.164	0.089	13.490	⋯
FSR 0749-1	05:32:32.83	41:35:53.28	2.5	−0.9	0.090	0.071	13.400	⋯
FSR 0816-1	05:38:48.06	31:31:58.17	1.5	−6.7	0.268	0.128	13.740	⋯
FSR 0799-1	05:42:32.10	33:28:59.98	−1.1	3.5	0.135	0.167	14.110	⋯
FSR 0904-1	06:06:59.26	19:02:46.91	−4.6	−7.6	0.111	0.131	12.450	⋯
Kronberger 12-1	06:14:17.82	22:25:30.87	−4.0	−4.1	0.269	0.153	12.840	⋯
Skiff J0619+18.5-13	06:18:28.07	18:29:22.94	−3.3	−1.8	0.293	0.150	13.720	⋯
Skiff J0619+18.5-12	06:18:29.97	18:36:18.94	4.8	−4.2	0.123	0.072	12.710	⋯
Skiff J0619+18.5-11	06:18:31.20	18:42:25.87	−7.2	−4.3	0.112	0.050	12.180	⋯
FSR 0902-1	06:19:04.97	20:35:21.87	−2.2	−5.3	0.172	0.033	12.690	⋯
Skiff J0619+18.5-2	06:19:12.04	18:29:47.52	−1.4	−2.3	0.042	0.107	11.840	⋯
Skiff J0619+18.5-3	06:19:20.08	18:13:23.20	−3.4	−3.5	0.016	0.088	11.740	⋯
Skiff J0619+18.5-4	06:19:36.38	18:25:41.62	−3.4	−0.2	0.187	0.134	12.870	⋯
Skiff J0619+18.5-5	06:19:51.87	18:12:52.66	−1.9	−6.2	0.237	0.110	13.080	⋯
Skiff J0619+18.5-1	06:20:01.00	18:36:26.38	−1.0	−0.1	0.079	0.111	12.170	⋯

Table 2
(Continued)

Object	R.A. (hh:mm:ss.ss)	Decl. (dd:mm:ss.ss)	$\mu_\alpha \cos\delta$ (mas yr^{-1})	μ_δ (mas yr^{-1})	$J-H$ (mag)	$H-K_s$ (mag)	R (mag)	SIMBAD
Dolidze 22-1	06:23:05.02	04:34:12.34	−3.9	−2.2	0.166	0.131	14.130	⋯
FSR 0955-1	06:23:50.30	14:30:55.57	2.0	−1.8	0.067	0.067	11.010	⋯
FSR 0955-2	06:24:01.29	14:29:43.15	−2.3	2.0	0.051	0.030	12.100	⋯
NGC 2244-1	06:32:43.48	04:51:21.50	−3.3	1.8	0.116	0.109	12.240	iC
FSR 0905-4	06:33:41.74	22:16:19.56	2.3	−9.1	0.092	0.053	13.260	⋯
FSR 0905-1	06:33:49.13	22:16:37.40	3.1	−7.1	0.116	0.030	12.150	⋯
FSR 0905-2	06:33:51.78	22:18:41.66	−0.7	−7.1	0.166	0.037	13.010	⋯
Basel 8-1	06:34:41.48	07:56:42.26	0.7	−2.0	0.110	0.056	11.660	⋯
Basel 8-3	06:34:57.09	08:10:55.74	−0.6	−3.9	0.067	0.136	12.770	⋯
Basel 8-2	06:35:38.31	08:04:13.36	−8.2	0.1	0.045	0.075	11.450	iC
Collinder 110-3	06:37:58.50	02:16:29.16	4.9	0.9	0.263	0.184	14.770	⋯
Collinder 110-2	06:38:24.54	02:17:05.31	3.3	−0.3	0.174	0.068	14.040	⋯
Collinder 110-1	06:38:38.27	02:13:36.76	4.6	−1.6	0.266	0.137	13.970	iC
Collinder 110-5	06:38:49.79	02:08:48.72	0.2	−1.0	0.172	0.139	14.320	iC
Collinder 110-4	06:38:54.16	02:11:57.40	0.9	−0.6	0.204	0.150	14.010	⋯
Collinder 110-12	06:38:55.36	01:57:02.14	−5.2	−6.0	0.214	0.133	14.190	iC
Collinder 110-6	06:39:22.49	01:49:33.72	7.0	−0.1	0.320	0.180	14.420	⋯
NGC 6866-12	20:03:04.09	44:14:15.69	−4.6	−3.3	0.082	0.041	12.600	⋯
NGC 6866-1	20:03:22.23	44:16:57.64	−3.4	1.9	0.047	0.083	12.110	iC
NGC 6866-2	20:03:49.51	44:10:50.70	−1.6	−3.9	0.050	0.049	12.150	iC
NGC 6866-3	20:03:56.83	44:10:31.90	−4.0	−5.8	0.073	0.029	12.120	⋯
NGC 6910-1	20:22:07.18	40:48:39.95	−3.4	0.4	0.208	0.120	12.360	iC
FSR 0253-2	21:02:33.46	39:53:13.80	3.2	−2.0	0.140	0.122	11.880	iC
FSR 0253-6	21:03:15.26	39:56:36.24	−10.1	−5.2	0.214	0.144	12.850	⋯
FSR 0253-1	21:03:23.05	39:59:17.95	4.5	−0.4	0.075	0.107	11.100	⋯
FSR 0253-5	21:03:27.60	40:05:44.89	−9.9	0.4	0.213	0.196	13.180	⋯
FSR 0253-4	21:03:28.38	40:08:46.48	−4.5	2.7	0.177	0.136	13.320	⋯
FSR 0253-7	21:03:57.98	40:10:09.00	−6.0	−3.6	0.335	0.215	14.050	⋯
FSR 0253-3	21:03:59.37	40:01:08.51	−4.6	−2.1	0.207	0.098	12.610	⋯
FSR 0354-1	22:10:51.21	57:49:33.71	−9.0	−3.5	0.298	0.311	11.610	Em
FSR 0354-2	22:12:13.56	57:39:37.34	−1.8	3.0	0.275	0.302	11.480	⋯
NGC 7654-1*	23:24:21.86	61:29:21.08	−3.1	−6.5	0.132	0.240	11.590	Em
NGC 7654-2*	23:24:46.38	61:26:15.41	−8.7	3.0	0.179	0.219	11.090	Be (B9)

Note. Column 1: Names of Be star candidates. Names with an asterisk are objects reported in WEBDA. Column 2: Right Ascension (R.A.) in hms (J2000). Column 3: Declination (decl.) in hms (J2000). Column 4: Proper motion of R.A. Column 5: Proper motion of decl. Column 6: 2MASS $J-H$ colors. Column 7: 2MASS $H-K_s$ colors. Column 8: R-band magnitudes obtained from USNO-B and PTF/iPTF catalogue. Column 9: Object classification adopted from SIMBAD; Be: Be stars; iC: star in cluster; Em: emission-line stars.

J and K_s values along with the isochrone from bright toward faint K_s magnitudes in the color–magnitude diagram (CMD; blue-dashed lines in Figure 3(c)). The photometric membership is determined by selecting stars within the region that are near the isochrone (Girardi et al. 2002) for non-emission-line stars. However, Be stars could have unusually large infrared excess with $J-H$ and $H-K_s$ both being greater than 0.6 mag (Lee & Chen 2011). Therefore, we extended the selection region for the emission-line candidates with $J-K_s \sim 1.2$ mag (red-dashed lines in Figure 3(c)).

3.4. Identifying Kinematic Membership

After identification of photometric membership, kinematic information can be obtained to further secure the membership in a star cluster by PMs. We have calculated the averaged PM and standard deviations of stars within the searching region by fitting a Gaussian distribution to PMs $\mu\alpha$ and $\mu\beta$. The σ_μ is the error propagated from $\sigma_{\mu\alpha}$ and $\sigma_{\mu\beta}$, whereas $\sigma_{\mu\alpha}$ and $\sigma_{\mu\beta}$ are the standard deviations of $\mu\alpha$ and $\mu\beta$, respectively. To exclude stars with inconsistent or high PMs, stars are considered to be kinematic members if they are located inside the $2\sigma_\mu$ region. It should be noted that our 2σ approach is just an approximate method. Better models would be required to obtain more precise determinations of kinematic membership.

3.5. Identifying Be Star Candidates

We defined a region in the $J-H$ versus $H-K_s$ color–color diagram to identify possible Be star candidates from emission-line candidates under the assumption that Be stars have similar infrared colors. As shown in Figure 3(e), the gray-dashed region covers gray contours representing infrared colors of over 1000 Be stars from the literature (Zhang et al. 2005). We thus selected possible Be star candidates inside the gray-dashed region in the color–color diagram. In Figure 3(f), we show the spatial distribution of clusters and Be star candidates. In Table 2, we list the properties of the Be candidates.

3.6. Selecting B-type Stars

We adopted the absolute K_s-band magnitude range[13] of B-type stars (−3.04–1.07 mag; see also Pecaut et al. 2012;

[13] http://www.pas.rochester.edu/~emamajek/

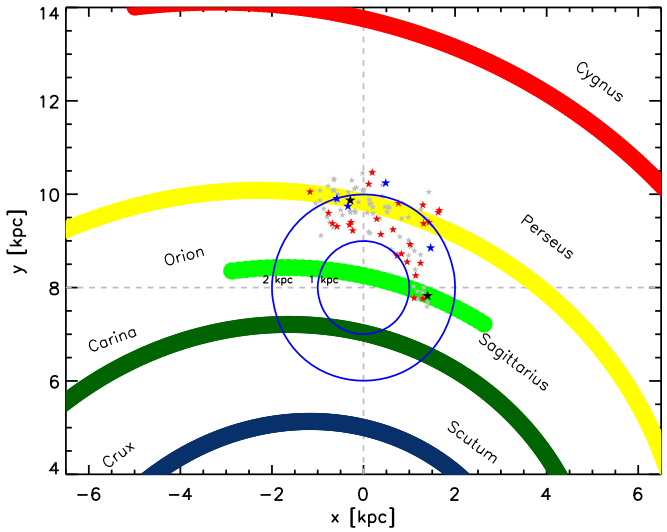

Figure 4. Cluster distribution in Galactic plane. Inner and outer blue circles represent 1 kpc and 2 kpc radii, respectively. Gray stars represent clusters with Be fraction = 0%; red stars show clusters with Be fraction <20%; blue stars depict clusters with Be fraction >20% and <40%; black stars show clusters with Be fraction >40%.

Pecaut & Mamajek 2013). For each cluster, we converted absolute magnitude to apparent magnitudes on the basis of their distance given by Kharchenko et al. (2013). Then we selected the stars that have apparent K_s-band magnitude within the range of B-type stars.

4. Results and Discussion

4.1. Clusters with Be Star Candidates

We discovered 85 Be star candidates in 27 clusters among 104 open clusters. The spatial distributions of the 104 clusters in the MW are shown in Figures 4 and 5. Most of the clusters are concentrated in the Galactic plane with latitude $|b| < 5°$. The clusters with Be candidates are not only located in spiral arms but also in the regions between arms. Most of clusters with the Be fraction N(Be)/N(Be+B-type) < 20% distribute randomly. However, clusters with Be star fraction N(Be)/N(Be +B-type) > 20% tend to be located in spiral arms (blue and black stars in Figure 4). Similarly, Mathew et al. (2008) showed that clusters possessing emission stars lie in the Perseus arm, indicating more active star formation. And yet it should be noted that these behaviors could change, as more data should be included to perform a statistical study. In Figure 6, among 32 clusters with Be star candidates, more than 50% of clusters have a Be fraction N(Be)/N(Be+B-type) less than 10%, which is consistent with previous studies (McSwain & Gies 2005; Mathew et al. 2008).

In Figure 7, we showed the fractions of clusters with Be star candidates as a function of age, which ranges from millions to billions of years. Each age bin shows a ratio of clusters with Be star candidates over all clusters within corresponding age. This ratio increases with age until $8.0 < \log(t(\mathrm{year})) \leqslant 8.5$, and then declines all the way to the oldest age bin (solid histogram in Figure 7). However, because our Hα data are limited to R-band magnitudes between ~11 and 16 mag, clusters with different distances would have different Be star completeness. We found that clusters with distance >1.5 kpc give the completeness of spectral type later than B5. Thus, if we only consider the clusters with distance >1.5 kpc, the peak of the ratios is in the bin of

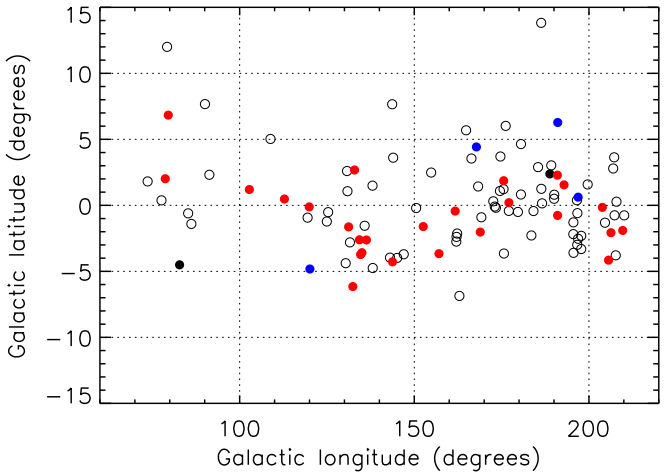

Figure 5. Cluster distribution in Galactic coordinates. Open circles: clusters with Be fraction = 0%; red filled circles: clusters with Be fraction <20%; blue filled circles: clusters with Be fraction >20% and <40%; black filled circles: clusters with Be fraction >40%.

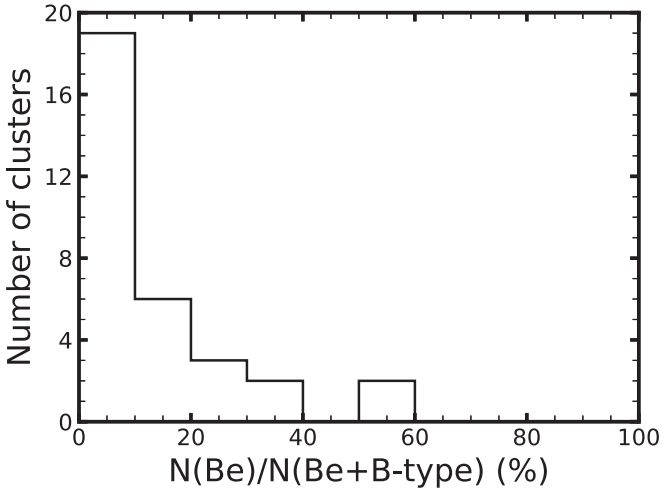

Figure 6. Fraction of clusters with Be star candidates. Most clusters have Be fraction <20%.

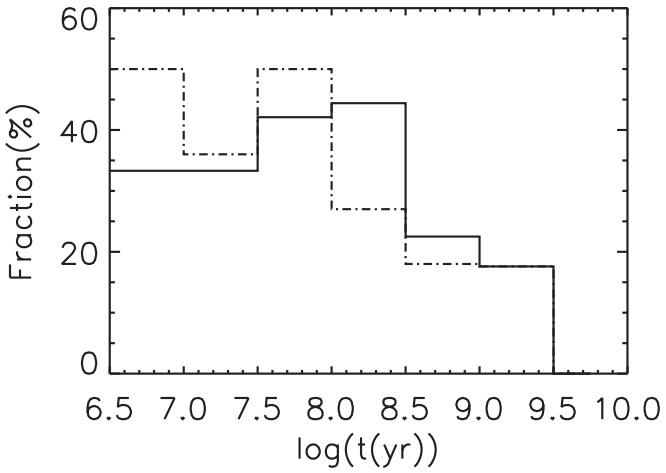

Figure 7. Fraction of clusters with Be star candidates. Solid lines: all clusters; dashed lines: clusters with distance >1.5 kpc. Clusters with age $7.5 < \log(t(\mathrm{year})) \leqslant 8.5$ tend to have Be star candidates.

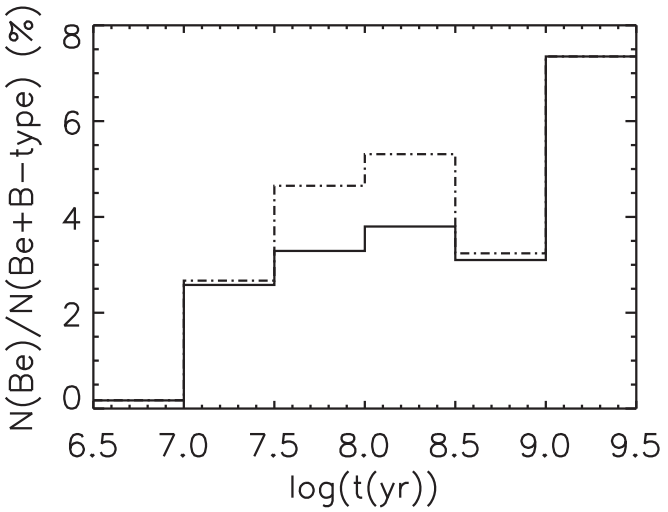

Figure 8. Be fraction N(Be)/N(Be+B-type) of clusters with different ages. Solid lines: all clusters; dashed lines: clusters with distance >1.5 kpc. Clusters within age bin of $7.5 < \log(t(\mathrm{year})) \leqslant 8.5$ tend to have a higher Be fraction N(Be)/N(Be+B-type).

$7.5 < \log(t(\mathrm{year})) \leqslant 8$ (dashed histogram in Figure 7). Although it seems that clusters with the age of $6.5 < \log(t(\mathrm{year})) \leqslant 7.0$ have higher value, we noted that this is caused by a small sample (only two clusters) in the bin. It is unlikely that the youngest clusters have a high probability of harboring Be stars, because they are mostly still in the pre-main sequence phase at this age.

4.2. Be Star Fraction versus Age

We compared the Be fraction N(Be)/N(Be+B-type) by summing all stars within the same age bin, e.g., each age bin shows a ratio of all Be star candidates to all B-types stars (Be +B-type). In Figure 8 (solid histogram), the ratio increases with ages and shows a peak at $8.0 < \log(t(\mathrm{year})) \leqslant 8.5$, then declines with older ages. As mentioned above, it is required to consider the clusters with distance >1.5 kpc to constrain the completeness. As shown in the dashed histogram in Figure 8, the fraction has a similar trend and the same peak as the original distribution. This result suggests that B-type stars with $7.5 < \log(t(\mathrm{year})) \leqslant 8.5$ tend to have more Be star candidates. On the other hand, it should be noted that the highest ratio seems to be in the oldest bin $9.0 < \log(t(\mathrm{year})) \leqslant 9.5$ at first glance. We examined those clusters older than $\log(t(\mathrm{year})) = 9$ and found that the main contribution of Be and B-type stars in this age bin is from cluster Collinder 110; it has 7 Be candidates and 47 B-type stars. If we remove this cluster, the Be fraction drops to ∼3%, which is lower than that of clusters with $7.0 < \log(t(\mathrm{year})) \leqslant 8.5$. The overabundance of Be star candidates in Collinder 110 should be further confirmed using spectroscopy.

To avoid the effects of extreme numbers of individual clusters, we averaged the Be fraction of clusters within the same age bin. In Figure 9, we showed the average of Be frequency as a function of cluster ages. The age index with $8.0 < \log(t(\mathrm{year})) \leqslant 8.5$ exhibits the highest mean Be fraction, and the fraction decreases toward the older cluster ages (filled circles in Figure 9). If we consider the completeness, the clusters with $7.5 < \log(t(\mathrm{year})) \leqslant 9$ have a high mean Be fraction (open diamond in Figure 9). For comparison, McSwain & Gies (2005) found the peak among clusters with $7.4 < \log(t(\mathrm{year})) < 8$, and Fabregat & Torrejón (2000) showed the peak is at $7.0 < \log(t(\mathrm{year})) < 7.4$. The

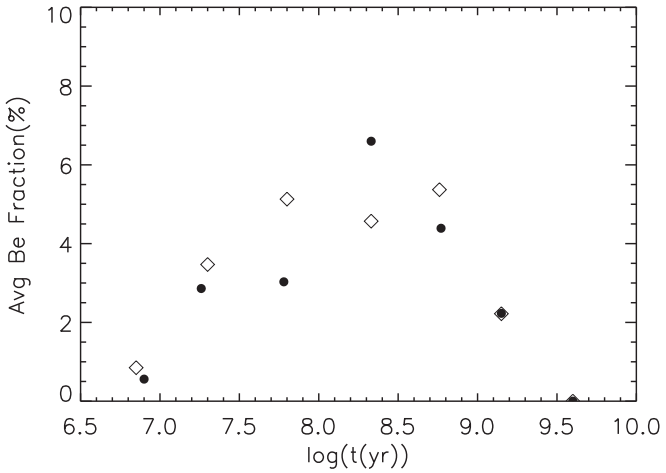

Figure 9. Averaged Be fraction N(Be)/N(Be+B-type) of clusters with different ages. Filled circles: all clusters; open diamonds: clusters with distance >1.5 kpc. The averaged Be fraction arises after the age of $\log(t(\mathrm{year})) = 7.5$ and then decreases after the age of $\log(t(\mathrm{year})) = 8.5$.

difference in these results is caused by different levels of completeness. Fabregat & Torrejón (2000) and McSwain & Gies (2005) have more complete early B-type stars, while we have a more complete sample of Be star candidates with spectral types later than B5.

4.3. Concentration of Be Star Candidates

The effects of mass segregation are essential in the dynamical evolution of open clusters, e.g., more massive stars are preferentially located in the central regions (Raboud & Mermilliod 1998; Littlefair et al. 2003; Chen et al. 2007). The effects are suggested to be caused by kinetic energy redistribution and equipartition (Bonnell & Davies 1998; de Grijs et al. 2002). Because Be stars are massive stars, the spatial distribution of Be stars in clusters with different ages might reveal the dynamical interaction snapshot among other members. Our cluster sample covers a wide range of ages from a few Myr to a few Gyr. We therefore investigate the concentration level with age by dividing the sample into young clusters ($7 < \log(t(\mathrm{year})) \leqslant 8$) and intermediate/old clusters ($8 < \log(t(\mathrm{year})) \leqslant 10$). Due to the small number of old clusters, we combine the samples of intermediate and old clusters. For each cluster, we estimated the Be star fraction N(Be)/N(Be+B-type) within four annuli; each annulus has a width of 1σ (Figure 10). The value σ is determined by fitting the radial density profile (see Section 3 and Figure 3). Then we averaged the Be star fraction within the same annulus of all clusters within the same age bin. In Figure 11, we show the average Be star fractions within different annuli. From the point of view of the cluster age, the Be fraction within the second annulus of the intermediate and old clusters is slightly higher than that of the young clusters within the same annulus. On the other hand, the clusters with intermediate ages have similar Be fractions to those of the young clusters within the other three annuli. However, either in the young or intermediate/old clusters, the Be star candidates distribute uniformly. The results might indicate that Be star candidates do not form preferentially in the central regions of clusters. A larger sample of clusters is crucial to conduct a statistical study and to test this hypothesis in the future.

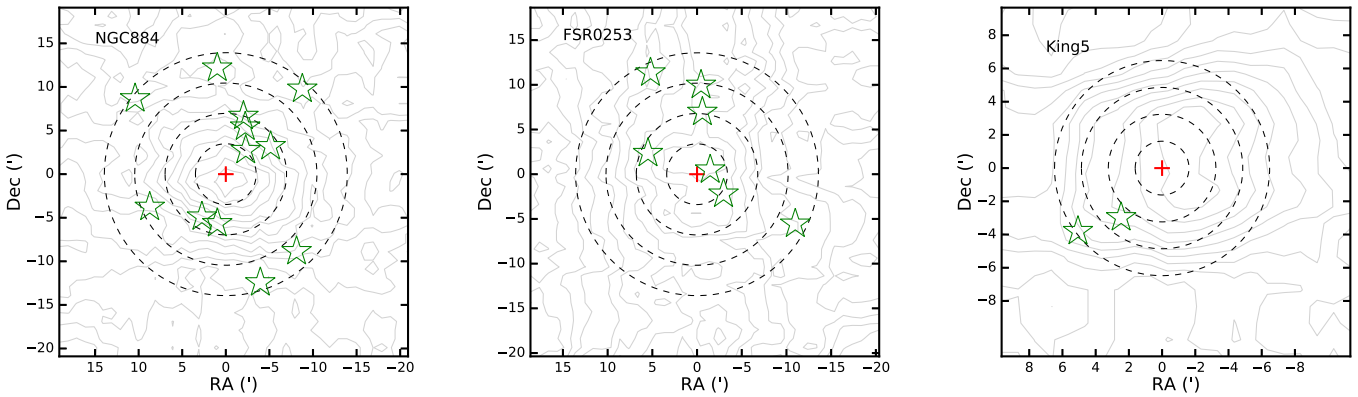

Figure 10. Examples of annulus definition for three clusters with different ages. Dashed circles represent the 1σ, 2σ, 3σ, and 4σ radii for each cluster. Green pentagrams are Be candidates.

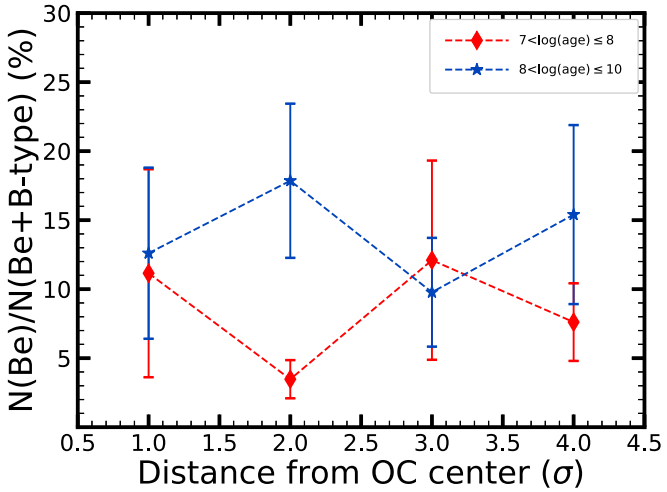

Figure 11. The concentration level of Be candidates. The lines with different colors show different age ranges. The Be fractions are the average ratios of Be/(Be+B-type) within the same age bin and annulus. Spatial distribution of Be star candidates with different ages suggests that the distribution is age-independent.

4.4. Infrared Colors

To further investigate infrared properties of Be candidates, we obtained the middle infrared (MIR) data from the *Wide-field Infrared Survey Explorer* (*WISE*; Wright et al. 2010) All-Sky Release.[14] The *WISE* mission has mapped the entire sky in four bands at 3.4, 4.6, 12, and 22 μm (hereafter called *W*1, *W*2, *W*3, and *W*4) with resolutions of 6.″1 and 6.″5 for *W*1, *W*2 and *W*3, and 12.″0 for *W*4. All four bands were imaged simultaneously, and the exposure times were 7.7 s in *W*1 and *W*2 and 8.8 s in *W*3 and *W*4. The data presented here have been calibrated with the *WISE* pipeline.

We performed photometry for these candidates on the *W*1, *W*2, *W*3, and *W*4 images and measured their integrated brightness using the method described in Hsia & Zhang (2014). After an initial inspection, we found that the detected S/N at *the W*4 band is very low for most candidates in our sample. We therefore limited our study to the objects in the searching range of *the W*1, *W*2, and *W*3 bands and restricted our sources to have S/N $>$ 4 in all three bands. To estimate the uncertainties in brightness, we adopt the standard deviations of all background-subtracted brightness measurements. The characteristic uncertainties of all brightness measurements are estimated to be ∼6%, 5%, and 21% for *W*1, *W*2, and *W*3 bands, respectively. In total, 61 Be star candidates have *W*1, *W*2, and *W*3 band data with sufficient S/N to study. A summary of *WISE* photometric results for the sources is given in Table 3, and their corresponding $W1-W2$ and $W2-W3$ color–color diagrams are shown in Figures 12 and 13.

In Figure 12, we compare their $W1-W2$ and $W2-W3$ colors with B type stars (Paunzen et al. 2005) and known Be stars (Zhang et al. 2005). More than 80% of our Be candidates are located around the upper-left of this color diagram. They also show similar color distributions as known Be stars, which is suggested to be caused by free–free emission or bound-free emission from proton-electron scattering (Chen et al. 2016). On the other hand, as noted by Chen et al. (2016), some Be stars located at the lower-right region might be indicative of the presence of circumstellar dust. However, none of our Be candidates are located in the lower-right region, suggesting their infrared excess are mainly due to free–free emission or bound-free emission.

The infrared color excess represents variations of circumstellar plasma or contribution from the ionized material. Dougherty et al. (1991) found that early type Be stars have larger IR color excesses than late type ones do, which are attributed to either dust emission or effect of photospheric emission by cool circumstellar disk. However, no correlation between *WISE* color and spectral type was found suggested by Chen et al. (2016).

To examine their age dependence, we plotted the $W1-W2$ versus $W2-W3$ diagram on the basis of their cluster ages. As shown in Figure 13, clearly, mid-infrared color excess are independent of the ages, indicating that the circumstellar material might not be correlated with their ages. Previous works also show relevant results about age independence of performance mainly in near-infrared, despite lack of sample clusters in different age. Wisniewski et al. (2007) presented imaging polarization observations of Be stars in the clusters of Magellanic Clouds. The Be stars in the youngest clusters show a really low IR color excess and distribute evenly as well as other candidates in the older clusters. On the other hand, a Be star with large IR excess still can be found in an older cluster of Magellanic Clouds reported by Paul et al. (2017). These works including ours indicated that NIR and MIR colors are not likely correlated with age, implying that the disk forming mechanisms, such as rapid rotation and pulsation, are not age dependent.

[14] http://wise2.ipac.caltech.edu/docs/release/allsky/

Table 3
WISE Photometric Data of Be Candidates

Object	3.4 μm (mag)	$\sigma_{3.4\,\mu m}$ (mag)	4.6 μm (mag)	$\sigma_{4.6\,\mu m}$ (mag)	12 μm (mag)	$\sigma_{12\,\mu m}$ (mag)	log(t(year))	$W1$–$W2$ (mag)	$W2$–$W3$ (mag)
Stock 20-1	10.708	0.023	10.733	0.021	10.425	0.122	8.337	−0.025	0.308
Stock 21-1	11.605	0.021	11.686	0.021	11.407	0.112	8.825	−0.081	0.279
Stock 21-2	12.288	0.023	12.309	0.023	12.006	0.173	8.825	−0.021	0.303
Stock 21-3	11.892	0.023	11.897	0.022	11.685	0.148	8.825	−0.005	0.212
NGC 743-1	9.174	0.022	8.822	0.021	7.901	0.019	8.290	0.352	0.921
NGC 743-2	10.988	0.023	11.015	0.020	11.125	0.127	8.290	−0.027	−0.110
NGC 743-3	10.972	0.023	10.993	0.021	11.154	0.125	8.290	−0.021	−0.161
NGC 743-4	10.783	0.023	10.657	0.021	10.041	0.064	8.290	0.126	0.616
NGC 744-1	10.934	0.023	10.961	0.022	10.990	0.127	8.375	−0.027	−0.029
NGC 744-5	11.538	0.022	11.565	0.022	11.688	0.252	8.375	−0.027	−0.123
NGC 744-13	9.958	0.023	9.961	0.021	9.861	0.045	8.375	−0.003	0.100
NGC 869-1	11.166	0.024	11.184	0.021	11.071	0.123	7.280	−0.018	0.113
NGC 869-2	11.071	0.024	11.095	0.021	11.503	0.175	7.280	−0.024	−0.408
NGC 869-3	12.225	0.024	12.276	0.023	⋯	⋯	7.280	−0.051	⋯
NGC 869-4	12.852	0.025	12.871	0.024	⋯	⋯	7.280	−0.019	⋯
NGC 869-14	10.754	0.023	10.780	0.021	10.873	0.108	7.280	−0.026	−0.093
NGC 869-15	10.831	0.022	10.855	0.022	11.002	0.109	7.280	−0.024	−0.147
NGC 869-16	11.024	0.023	11.035	0.020	11.028	0.116	7.280	−0.011	0.007
NGC 869-17	11.396	0.024	11.439	0.021	⋯	⋯	7.280	−0.043	⋯
NGC 869-18	12.112	0.023	12.123	0.023	⋯	⋯	7.280	−0.011	⋯
NGC 869-19	12.675	0.024	12.691	0.025	⋯	⋯	7.280	−0.016	⋯
NGC 869-20	12.943	0.024	12.969	0.025	⋯	⋯	7.280	−0.026	⋯
NGC 869-25	11.842	0.082	11.856	0.038	⋯	⋯	7.280	−0.014	⋯
NGC 869-26	10.281	0.071	10.008	0.021	9.073	0.030	7.280	0.273	0.935
NGC 869-27	10.512	0.023	10.255	0.020	9.395	0.034	7.280	0.257	0.860
Basel 10-1	9.807	0.023	9.534	0.021	8.780	0.029	7.600	0.273	0.754
NGC 886-1	10.455	0.024	10.171	0.020	9.188	0.034	8.750	0.284	0.983
NGC 884-1	10.150	0.023	10.176	0.020	9.809	0.045	7.200	−0.026	0.367
NGC 884-2	10.405	0.023	10.405	0.021	10.416	0.087	7.200	0.000	−0.011
NGC 884-3	11.446	0.023	11.453	0.023	11.350	0.150	7.200	−0.007	0.103
NGC 884-4	11.518	0.024	11.577	0.026	⋯	⋯	7.200	−0.059	⋯
NGC 884-5	11.381	0.024	11.400	0.021	11.390	0.143	7.200	−0.019	0.010
NGC 884-6	12.460	0.026	12.511	0.025	⋯	⋯	7.200	−0.051	⋯
NGC 884-8	11.169	0.024	11.255	0.023	⋯	⋯	7.200	−0.086	⋯
NGC 884-11	11.694	0.023	11.703	0.022	11.443	0.195	7.200	−0.009	0.260
NGC 884-12	12.000	0.128	12.134	0.022	10.343	0.091	7.200	−0.134	1.791
NGC 884-13	13.081	0.025	13.147	0.031	⋯	⋯	7.200	−0.066	⋯
NGC 884-14	12.675	0.024	12.691	0.025	⋯	⋯	7.200	−0.016	⋯
NGC 884-19	10.512	0.023	10.255	0.020	9.395	0.034	7.200	0.257	0.860
NGC 957-1	9.974	0.023	9.783	0.020	9.412	0.036	7.250	0.191	0.371
King 5-1	12.441	0.023	12.452	0.024	⋯	⋯	9.090	−0.011	⋯
King 5-2	12.228	0.023	12.215	0.024	⋯	⋯	9.090	0.013	⋯
NGC 1513-1	11.002	0.023	11.011	0.021	10.883	0.111	8.500	−0.009	0.128
NGC 1513-2	11.511	0.022	11.535	0.021	⋯	⋯	8.500	−0.024	⋯
NGC 1513-3	11.647	0.023	11.626	0.023	11.711	0.240	8.500	0.021	−0.085
Berkeley 1-1	12.081	0.024	12.073	0.023	11.718	0.253	8.700	0.008	0.355
NGC 1664-1	11.541	0.023	11.547	0.021	11.739	0.248	8.750	−0.006	−0.192
NGC 1778-1	10.419	0.023	10.317	0.020	9.715	0.050	8.450	0.102	0.602
FSR 0749-1	12.168	0.023	12.173	0.024	⋯	⋯	8.620	−0.005	⋯
FSR 0749-2	11.850	0.023	11.872	0.022	⋯	⋯	8.620	−0.022	⋯
FSR 0799-1	12.465	0.024	12.367	0.025	11.711	0.259	9.095	0.098	0.656
FSR 0816-1	12.575	0.025	12.574	0.027	⋯	⋯	7.800	0.001	⋯
FSR 0904-1	10.581	0.024	10.322	0.021	9.552	0.058	7.800	0.259	0.770
Kronberger 12-1	11.825	0.023	11.803	0.025	⋯	⋯	8.870	0.022	⋯
FSR 0902-1	11.381	0.022	11.409	0.022	10.723	0.251	7.145	−0.028	0.686
Skiff J0619+18.5-1	11.277	0.024	11.316	0.022	10.677	0.110	7.900	−0.039	0.639
Skiff J0619+18.5-2	10.957	0.026	10.988	0.024	10.984	0.200	7.900	−0.031	0.004
Skiff J0619+18.5-3	11.159	0.024	11.174	0.022	11.313	0.181	7.900	−0.015	−0.139
Skiff J0619+18.5-4	11.495	0.023	11.483	0.022	11.400	0.187	7.900	0.012	0.083
Skiff J0619+18.5-5	11.403	0.024	11.382	0.022	11.338	0.223	7.900	0.021	0.044
Skiff J0619+18.5-11	11.223	0.023	11.240	0.022	11.140	0.139	7.900	−0.017	0.100
Skiff J0619+18.5-12	11.682	0.024	11.708	0.023	⋯	⋯	7.900	−0.026	⋯
Skiff J0619+18.5-13	11.818	0.023	11.813	0.023	⋯	⋯	7.900	0.005	⋯

Table 3
(Continued)

Object	3.4 μm (mag)	$\sigma_{3.4\,\mu m}$ (mag)	4.6 μm (mag)	$\sigma_{4.6\,\mu m}$ (mag)	12 μm (mag)	$\sigma_{12\,\mu m}$ (mag)	log(t(year))	$W1-W2$ (mag)	$W2-W3$ (mag)
Dolidze 22-1	12.407	0.023	12.441	0.023	⋯	⋯	8.370	−0.034	⋯
FSR 0955-1	10.275	0.024	10.300	0.020	10.265	0.092	7.400	−0.025	0.035
FSR 0955-2	11.391	0.024	11.405	0.022	11.631	0.267	7.400	−0.014	−0.226
NGC 2244-1	11.183	0.025	11.225	0.024	⋯	⋯	6.700	−0.042	⋯
FSR 0905-1	11.261	0.024	11.289	0.022	⋯	⋯	8.300	−0.028	⋯
FSR 0905-2	12.239	0.024	12.206	0.029	⋯	⋯	8.300	0.033	⋯
FSR 0905-4	12.416	0.025	12.427	0.029	⋯	⋯	8.300	−0.011	⋯
Basel 8-1	10.765	0.022	10.770	0.020	10.657	0.142	7.925	−0.005	0.113
Basel 8-2	10.691	0.022	10.716	0.021	11.214	0.259	7.925	−0.025	−0.498
Basel 8-3	11.875	0.023	11.927	0.023	⋯	⋯	7.925	−0.052	⋯
Collinder 110-1	12.212	0.024	12.202	0.025	⋯	⋯	9.220	0.010	⋯
Collinder 110-2	12.929	0.024	12.957	0.028	⋯	⋯	9.220	−0.028	⋯
Collinder 110-3	13.068	0.026	13.066	0.033	⋯	⋯	9.220	0.002	⋯
Collinder 110-4	12.342	0.024	12.324	0.023	⋯	⋯	9.220	0.018	⋯
Collinder 110-5	12.893	0.024	12.946	0.029	⋯	⋯	9.220	−0.053	⋯
Collinder 110-6	12.147	0.023	12.129	0.024	⋯	⋯	9.220	0.018	⋯
Collinder 110-12	12.669	0.024	12.685	0.027	⋯	⋯	9.220	−0.016	⋯
NGC 6866-1	11.452	0.023	11.479	0.022	⋯	⋯	8.640	−0.027	⋯
NGC 6866-2	11.506	0.023	11.552	0.021	11.785	0.224	8.640	−0.046	−0.233
NGC 6866-3	11.332	0.023	11.381	0.021	11.905	0.218	8.640	−0.049	−0.524
NGC 6866-12	11.781	0.023	11.810	0.022	11.125	0.127	8.640	−0.029	0.685
NGC 6910-1	10.900	0.023	10.903	0.020	9.967	0.109	7.530	−0.003	0.936
FSR 0253-1	10.235	0.022	10.274	0.020	10.266	0.062	8.275	−0.039	0.008
FSR 0253-2	10.689	0.023	10.707	0.020	10.348	0.054	8.275	−0.018	0.359
FSR 0253-3	11.611	0.023	11.640	0.021	11.313	0.140	8.275	−0.029	0.327
FSR 0253-4	11.952	0.023	11.965	0.022	12.061	0.224	8.275	−0.013	−0.096
FSR 0253-5	11.770	0.023	11.770	0.021	11.891	0.216	8.275	0.000	−0.121
FSR 0253-6	11.831	0.023	11.875	0.021	12.020	0.246	8.275	−0.044	−0.145
FSR 0253-7	11.528	0.023	11.505	0.021	11.905	0.184	8.275	0.023	−0.400
FSR 0354-1	9.364	0.023	9.062	0.020	8.111	0.021	8.000	0.302	0.951
FSR 0354-2	9.300	0.022	8.895	0.019	7.948	0.018	8.000	0.405	0.947
NGC 7654-1	10.455	0.023	10.260	0.021	9.495	0.035	7.900	0.195	0.765
NGC 7654-2	10.093	0.022	9.942	0.020	9.086	0.027	7.900	0.151	0.856

Note. Column 1: Names of Be candidates. Column 2: Magnitudes of the $W1$ band. Column 3: Uncertainties of the $W1$ band. Column 4: Magnitudes of the $W2$ band. Column 5: Uncertainties of the $W2$ band. Column 6: Magnitudes of the $W3$ band. Column 7: Uncertainties of the $W3$ band. Column 8: Ages of host clusters. Column 9: $W1-W2$. Column 10: $W2-W3$.

4.5. Optical Variability

Be stars exhibit photometric and spectroscopic variability with various timescales of days to years (Hubert et al. 1997; Hubert & Floquet 1998; Percy et al. 2002; Kourniotis et al. 2014; Labadie-Bartz et al. 2017). It has been suggested that Be stars have different phases of the circumstellar disk, such as ejecting material from the stellar surface, disk growth, and dissipation, which could cause variability. While outbursts or variability on short and intermediate timescales of days to months are believed to be caused by non-radial pulsation, ejected material or stellar winds, the variability with long timescales of years to decades is associated with the appearance and disappearance of the disk or the global density oscillations (Okazaki 1997; Labadie-Bartz et al. 2017). Therefore, investigating long-term variability of Be stars in different environments could provide us with insight into their disk evolution. Investigating short-term and mid-term variability requires the survey with high cadences of hours and days. The current catalogs, with lower cadences of days to weeks or months, are more beneficial for studying long-term variability. Thus, we study long-term variability (>200–300 days) for our Be star candidates in this work.

Time windows of the All Sky Automated Survey (ASAS[15]; Pojmanski 1997) and PTF/iPTF allow us to investigate the long-term variability of Be star candidates. We adopted the ASAS data to investigate the variability for Be star candidates with R-band magnitudes brighter than 14. The ASAS surveyed the available sky south of decl. +28° using I (ASAS-2, from 1998 to 2000) and V (ASAS-3, from 2000 to 2009) band filters with a $8\overset{\circ}{.}5 \times 8\overset{\circ}{.}5$ field of view. We used ASAS-3 database[16] to search for the V-band variability of Be star candidates (see also Pojmański 2001). We used the search radius of 5″ and only selected the data that is marked with "A" in the grade flag of the catalog, indicating the best data, to ensure that the photometry is convincing. Twenty-one of our Be candidates can be found in the ASAS-3 catalog.

On the other hand, PTF R-band data were adopted to investigate the variability of Be star candidates with R-band fainter than 14 mag. We used the search radius of 3″ and selected observations with the "ipac" flag marked with 0 and with the "SEXtractor" flag $\leqslant 2$ in the catalog to ensure that the data qualify as reliable. We also neglected the sources that only

[15] http://www.astrouw.edu.pl/asas/
[16] http://www.astrouw.edu.pl/asas/?page=aasc&catsrc=asas3

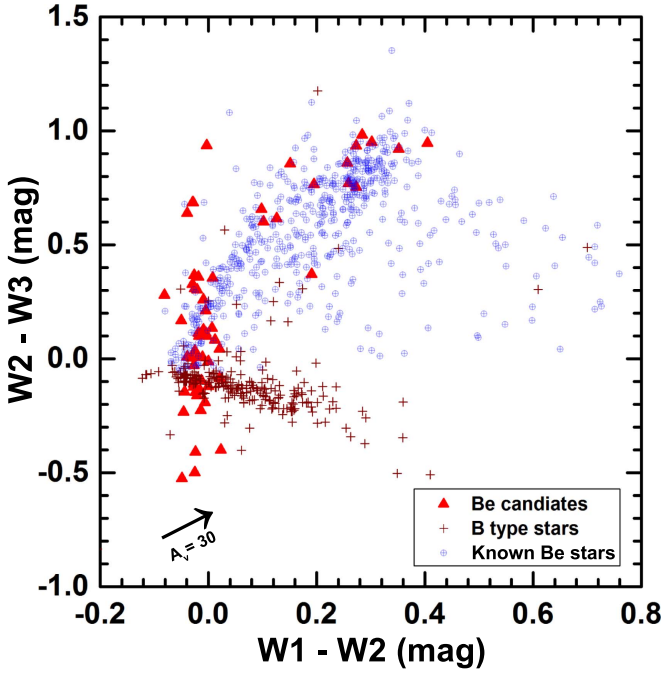

Figure 12. *WISE* *W*1–*W*2 vs. *W*2–*W*3 color–color diagram for studied cluster Be star candidates. Also plotted are 224 normal B type stars (brown crosses; Paunzen et al. 2005) and 538 known Be stars (blue circles; Zhang et al. 2005) with these Be star candidates of our sample (red triangles). Note that the MIR distribution of Be star candidates in our sample is similar to that of known Be stars.

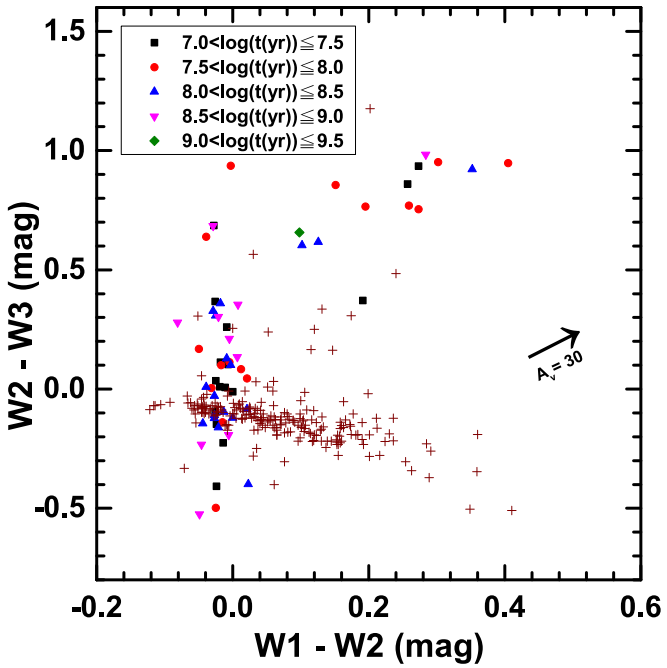

Figure 13. *WISE* *W*1–*W*2 vs. *W*2–*W*3 color–color diagram for studied Be star candidates with different ages (blue and pink triangles, black squares, red circles, and green diamonds) plus normal B type stars (brown crosses; Paunzen et al. 2005) for comparison. The distributions of our Be star candidates are not related to their ages.

have data points less than 10 observations. In total, 10 Be star candidates are selected from the PTF catalogue.

By applying differential photometry, among 31 Be star candidates with qualified photometric data points, we found that no Be star candidates have long-term variability within a

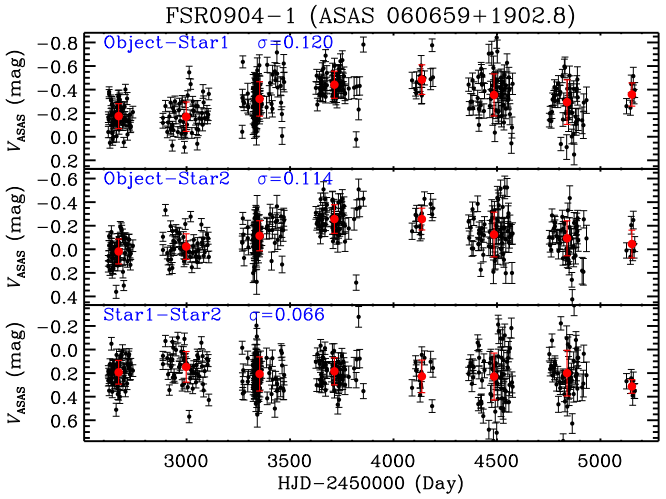

Figure 14. Differential photometry of the Be star candidate FSR 0904-1 and its comparison stars. The upper and middle panels show the differential light curves between FSR 0904-1 and its two comparison stars, ASAS 060659+1902.8 and ASAS 060649+1901.2, respectively. The lower panel shows the differential light curve between the two comparison stars. The error-weighted mean of each epoch is represented by red dot. FSR 0904-1 exhibits greater variation (σ = 0.120 and 0.114) than its comparison stars (σ = 0.066).

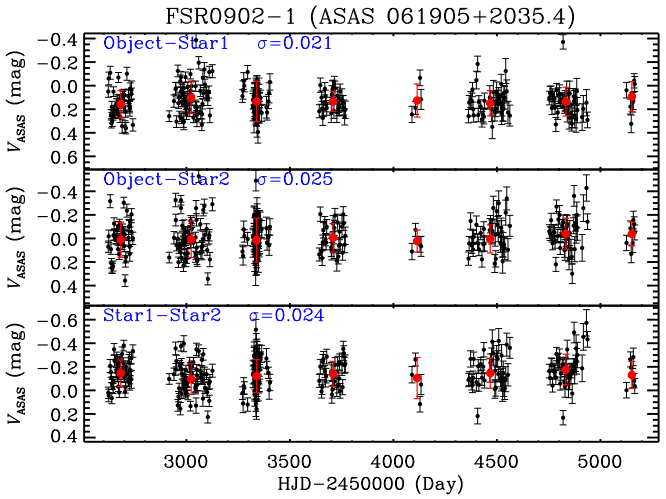

Figure 15. Differential photometry of the Be star candidate FSR 0902-1 and its comparison stars ASAS 061829+2025.9 and ASAS 061917+2038.8. FSR 0902-1 shows similar variation with its comparison stars, indicating that it has no variability.

timescale of several hundred days. However, we discovered that one Be candidate FSR 0904-1 shows prominent long-term variability, with an amplitude of 0.2–0.3 mag on a longer timescale of ∼2000 days. The differential photometry among the object FSR 0904-1 and two nearby comparison stars with similar brightness are shown in Figure 14. We estimated the mean photometric scatters of different epochs; while the Be candidate FSR 0904-1 has larger variation (σ = 0.120 and 0.114), comparison stars show smaller variations (σ = 0.066), suggesting the Be candidate FSR 0904-1 has possible long-term variability. For comparison, the differential light curve of Be candidate FSR 0902-1, with no obvious long-term variability, is shown in Figure 15.

Mennickent et al. (2002) found that Be star candidates have four types of light curves. Type-1 stars show sharp or hump-like outbursts with a mean timescale of 126 days that could be

similar to the outbursting reported by Hubert & Floquet (1998). Type-2 stars have sudden brightness increasing with an amplitude of a few tenths of magnitude, and remain a similar brightness for hundreds of days. High and low states are usually observed in type-2 Be star candidates. Type-3 Be star candidates show periodic or quasi-period oscillations, and type-4 stars exhibit random variability on timescales of days to years. Sabogal et al. (2014) conducted a search for southern Galactic Be star candidates within the ASAS catalog; they found that only 9% of Be star candidates show outburst (Type-1 stars) while 91% of the candidates show random variations (Type-4 stars). Nevertheless, none of the Be star candidates reported by these studies show the similar long-term variations of FSR 0904-1.

Several possibilities might cause these kind of long-term variations. One possibility is the contamination of nearby stars due to poor angular resolution ($\sim 14''$) of the ASAS survey. However, after examining PTF *R*-band images, we have ruled out this possibility. No nearby stars are located at the $15'' \times 15''$ region of the Be candidate FSR 0904-1. The other possibility is a long-lived strong outburst. The timescale of a long-term outburst, however, is usually 200–300 days (Hubert & Floquet 1998). The long timescale of FSR 0904-1 variation is unlikely related to an outburst. Another possibility is the global density oscillations in the circumstellar disk (Haubois et al. 2012). As shown in Labadie-Bartz et al. (2017), they found that some Be stars also have similar long-term variability, on the timescale of 2000–3000 days. Using simultaneous spectroscopic observations, they suggested that the global density oscillations could cause the long-term variability observed in brightness change and violet-to red ratio (V/R) of the Hα line. Unfortunately, we are unable to test this hypothesis without simultaneous time-series spectroscopic measurements. However, the photometric variability usually has a positive relation with the variability of the Hα emission-line strength, which originated from the circumstellar disk. Thus, the long-term timescale of photometric variability also implies that the timescale of the disk evolution might be as long as $\sim$2000 days.

5. Summary and Conclusions

We identified 96 Be star candidates in about 31% of the clusters (32/104). The clusters with a high Be fraction N(Be)/N(Be+B-type) $> 20\%$ tend to be located in spiral arms, which could indicate active star formation. More than half of the clusters with Be star candidates have Be fraction N(Be)/N(Be +B-type) $< 10\%$, which is similar to previous studies. We found that clusters with age $7.5 < \log(t(\mathrm{year})) \leqslant 8.5$ tend to have Be star candidates. Also, clusters with age $7.5 < \log(t(\mathrm{year})) \leqslant 8.5$ have higher Be fraction N(Be)/N(Be+B-type). These results suggest that environments of young ($\sim$30 Myr) and intermediate ($\sim$300 Myr) clusters could be beneficial to the formation of Be stars. We compared the concentration level of Be star candidates with different ages. We found that the Be star candidates in either young or old clusters are not centrally concentrated in the clusters. This implies that Be stars do not form preferentially in the central regions of clusters. We showed that Be star candidates have similar MIR colors to the known Be stars, and their MIR color excesses are independent of the ages. If the MIR color excesses are mainly due to free–free or bound-free emission from the material of the circumstellar disk, this result indicates that the material might not correlate with their ages. Finally, we discovered that one Be candidate, FSR 0904-1, shows long-term variability with an amplitude of 0.2–0.3 mag on the timescale of $\sim$2000 days. The long-term timescale of the variability implies the timescale of disk evolution might be $\sim$2000 days.

This work is supported in part by the Ministry of Science and Technology of Taiwan under grants MOST 105-2119-M-008-003 (W.-H.I.), MOST 103-2112-M-008-024-MY3 (W.-P.C.), MOST 104-2112-M-008-012-MY3 (C.-C.N.), MOST 104-2112-M-008-014-MY3 (C.-K.C), and MOST 106-2917-I-564-042 (C.-C.L.). This work is also supported by the Science and Technology Development Fund of Macau (project codes: 039/2013/A2 and 017/2014/A1). This publication makes use of data products from the Two Micron All Sky Survey, which is a joint project of the University of Massachusetts and the Infrared Processing and Analysis Center/California Institute of Technology, funded by the National Aeronautics and Space Administration and the National Science Foundation. This publication makes use of data products from the *Wide-field Infrared Survey Explorer*, which is a joint project of the University of California, Los Angeles, and the Jet Propulsion Laboratory/California Institute of Technology, funded by the National Aeronautics and Space Administration. This research has made use of the WEBDA database, operated at the Department of Theoretical Physics and Astrophysics of the Masaryk University.

Appendix
Notes of Individual Clusters

Basel 10: We identified one Be candidate in this cluster. Kharchenko et al. (2012) used NIR CMD and used the age of turn-off stars to calculate some parameters of this cluster. The distance and age are 2 kpc and $\sim$4 Myr, respectively, which are similar to those of Gozha et al. (2012) (1944 pc and $10^{7.6}$ year). Mermilliod et al. (2008) used the spectroscopic method to calculate the mean radial velocity of this cluster and one member of the cluster.

Berkeley 11: We identified one Be candidate in this cluster. Kharchenko et al. (2012) determined that the distance and age are 1.9 kpc and 50 Myr, respectively. Dias et al. (2014) identified 79 member stars in this cluster. Leisawitz et al. (1989) conducted a CO survey for 34 open clusters, and they found that molecular clouds are located within/around this cluster.

Dolidze 22: We identified one Be candidate in this cluster. The results of distance and age are 1.7 kpc and 234 Myr, respectively (Kharchenko et al. 2012). Dias et al. (2014) have identified 445 member stars in this cluster.

NGC 2244: We identified one Be star candidate in this cluster. This cluster is located in a giant molecular clouds Rosette nebula (Wang et al. 2008). Many Herbig Ae/Be stars are found in this young massive cluster. Banerjee & Kroupa (2017) used *N*-body simulations to study the cluster size of young massive clusters. They found that the simulated results were much more compact than observed one. There might be some additional mechanisms that affect the expansion of massive clusters.

NGC 869: We identified 14 Be star candidates in this cluster. Mathew & Subramaniam (2011) used spectroscopic observations to identify 6 Be stars while Marsh Boyer et al. (2012)

reported 15 Be stars in this cluster. The V/R ratio of one of our Be star candidates (NGC 869-26) was found to change from multiple observations during 2006 and 2007, indicating the turbulent nature of the circumstellar disk (Mathew & Subramaniam 2011). Pan et al. (2016) used BV photometry for an EB-type eclipsing binary and determined the mass ratio was 0.05 ± 0.001. The results suggest that the secondary component could be a giant or subgiant star with the outer envelope being stripped.

NGC 884: NGC 884 and NGC 869 could be a binary system of clusters. We identified 12 Be star candidates in this cluster. While Marsh Boyer et al. (2012) identified 13 Be stars in the cluster, Mathew & Subramaniam (2011) found that one Be star (NGC 884-1) showed spectroscopic variability with a period of 23 months. Using photometric measurements and membership probability, Ahumada & Lapasset (1995) identified one blue straggler in NGC 884.

NGC 957: We identified one Be star candidate, which is also listed on WEBDA. Schild & Romanishin (1976) discovered four Be stars while Mathew et al. (2008) have identified two Be stars in NGC 957. Kharchenko et al. (2012) found the distance of NGC 957 to be 1.9 kpc, which is similar to that found by Gimenez & Garcia-Pelayo (1980, 1.85 kpc).

Kronberger 12: We identified one Be candidate in this cluster. Using morphologies, CMD, and stellar density distribution, this cluster was identified as a possible open cluster by Kronberger et al. (2006). Despite a small amount of hot stars, it is one of the two clusters with the highest Be fraction. Our estimation cluster size is about 8′, which is several times larger than the visual size reported form the literature (Dias et al. 2002; Kronberger et al. 2006).

FSR 0749: Two Be candidates that we identified in this old cluster are not catalogued yet in SIMBAD. With a new developed method called the foreground-star-counting technique (Buckner & Froebrich 2013), the estimated cluster distance and *H*-band extinction are 2.9 kpc and 0.1 mag.

NGC 1220: Using *UBV* photometric observations, Ortolani et al. (2002) argued that NGC 1220 is a young compact cluster with an age of 60 Myr and a distance of 1800+/−200 pc. We found the cluster has a radius of 2.2 arcmin, which is similar to that found by Ortolani et al. (2002). Comparing to Kharchenko et al. (2013), they showed that NGC 1220 has an elder age of about 158 Myr and a distance of 2100 pc. In this work, we did not find Be star candidates for this cluster. However, Mathew & Subramaniam (2011) spectroscopically confirmed one Be star with the B5 spectral type in this cluster.

NGC 1348: This is a poorly known open cluster. Carraro (2002) showed that the cluster has a similar distance, 1.9 kpc, to that of Kharchenko et al. (2013). Recently, Fang et al. (2012) discovered an active eclipsing binary in the field of NGC 1348. We found no Be star candidates in this cluster.

NGC 1907: NGC 1907 and NGC 1912 are suggested as a binary cluster due to their similar distance (Subramaniam et al. 1995). However, Lee & Lee (1996) argued that their distance and age difference is so large that they are not physically connected. From orbital motions derived from a Galactic potential model and *N*-body simulations, de Oliveira et al. (2002) suggested that the clusters were born in different regions of the Galaxy and the pair is just a close encounter. No Be stars/candidates were reported in the cluster.

NGC 2269: Kharchenko et al. (2013) obtained a similar distance (1.58 kpc) to that found by Moffat & Vogt (1975, 1.44 kpc). With an age of 457 Myr, we reported no Be star candidatess in this cluster.

Berkeley 17: With an age of (∼10 Gyr), the cluster is the oldest cluster in our sample. No Be or B-type stars were found in our study of this cluster. It also could be the oldest known open cluster (Salaris et al. 2004). A tail-like structure can be detected with either 2MASS or Pan-STARRS data (Chen et al. 2004; Bhattacharya et al. 2017). Recently, Bhattacharya et al. (2017) discovered more massive than low-mass members in the core, suggesting the cluster should have a mass segregation effect.

FSR 0904: We found one Be star candidate in the cluster. FSR 0904 is a cluster candidate with an age of 6.3 Myr and a distance of 1.43 kpc (Kharchenko et al. 2013). Buckner & Froebrich (2016) studied 13 FSR clusters and indicated that the cluster should be younger than 80 Myr, which is consistent with Kharchenko et al. (2013).

SAI 24: The cluster was identified by Glushkova et al. (2010, see also Collinder 34 in Saurin et al. 2015). The cluster is in a star-forming region associated with Cas OB6. It is a young cluster with an age of 15 Myr, and we found no Be star candidates in this cluster.

NGC 744: Three Be candidates were identified as cluster members; two of them are catalogued in SIMBAD known as TYC 3688-1659-1 and TYC 3688-1741-1. Leisawitz et al. (1989) reported four foreground molecular clouds possibly associated with NGC 744.

NGC 743: Our estimation of cluster angular size is nearly 1° across. This loose cluster had the largest angular size. It harbors the greatest amount of B type stars among billion-year-old clusters. We found four emission-line candidates in which GGA 134 is a known emission-line star (González & González 1954).

NGC 886: This is one of the oldest clusters in our sample. We identified one Be candidate from the cluster members. It was also reported as an emission-line candidate, VES 734 (Coyne & MacConnell 1983). The cluster mass within tidal radius is about 400 solar masses (Piskunov et al. 2008).

NGC 1513: We found three cluster members as Be candidates. They are first reported by del Rio & Huestamendia (1988) and catalogued in SIMBAD. Two Be candidates, NGC 1513 RH 27 and NGC 1513 RH 47, have a high membership possibility up to 90% estimated by Frolov et al. (2002).

NGC 1664: The mass of this old cluster is about 1000 solar masses (Piskunov et al. 2008). We identified one Be candidate known as TYC 2906-590-1 in SIMBAD. Recently, van Cauteren et al. (2005) searched variables in this cluster, and two confirmed variable stars with δ Scuti-like light curves are reported.

NGC 6866: This cluster is in the Cygnus within the *Kepler* field but there are no Be stars reported in the literature. In 2013, LAMOST obtained 10000 spectra from NGC 6866 (Ren et al. 2016). It will be necessary to further confirm and analyze the photometric and spectroscopic variability of our four Be candidates in this region.

FSR 0253: This cluster not only hosts many Be candidates but has a high Be fraction. We identified 7 Be candidates out of 14 B type stars. In our cluster sample, only two reach such a high Be fraction. However, the other one (Kronberger 12) only has one Be candidate. One Cepheids, VY Cyg, has a probable

photometric and kinematic relation to FSR 0253 reported by Glushkova et al. (2015).

ORCID iDs

Po-Chieh Yu (俞伯傑) https://orcid.org/0000-0001-8894-0854
Chien-De Lee (李建德) https://orcid.org/0000-0002-3142-7299
I-Chenn Chen (陳以忱) https://orcid.org/0000-0002-1497-9884
Chow-Choong Ngeow (饒兆聰) https://orcid.org/0000-0001-8771-7554
Wen-Ping Chen (陳文屏) https://orcid.org/0000-0003-0262-272X
Jason Surace https://orcid.org/0000-0001-7291-0087
Shrinivas R. Kulkarni https://orcid.org/0000-0001-5390-8563

References

Ahumada, J., & Lapasset, E. 1995, A&AS, 109, 375
Allen, D. A. 1973, MNRAS, 161, 145
Banerjee, S., & Kroupa, P. 2017, A&A, 597, A28
Barbon, R., & Hassan, S. M. 1973, A&AS, 10, 1
Barnsley, R. M., & Steele, I. A. 2013, A&A, 556, A81
Bessell, M. S., & Brett, J. M. 1988, PASP, 100, 1134
Bhattacharya, S., Mishra, I., Vaidya, K., & Chen, W.-P. 2017, ApJ, 847, 138
Bonnell, I. A., & Davies, M. B. 1998, MNRAS, 295, 691
Buckner, A. S. M., & Froebrich, D. 2013, MNRAS, 436, 1465
Buckner, A. S. M., & Froebrich, D. 2016, arXiv:1611.03753
Carciofi, A. C., Okazaki, A. T., Le Bouquin, J.-B., et al. 2009, A&A, 504, 915
Carraro, G. 2002, A&A, 387, 479
Chen, L., de Grijs, R., & Zhao, J. L. 2007, AJ, 134, 1368
Chen, P. S., Liu, J. Y., & Shan, H. G. 2016, MNRAS, 463, 1162
Chen, W. P., Chen, C. W., & Shu, C. G. 2004, AJ, 128, 2306
Chojnowski, S. D., Whelan, D. G., Wisniewski, J. P., et al. 2015, AJ, 149, 7
Chojnowski, S. D., Wisniewski, J. P., Whelan, D. G., et al. 2017, AJ, 153, 174
Coyne, G. V., & MacConnell, D. J. 1983, VatOP, 2, 73
Cui, X.-Q., Zhao, Y.-H., Chu, Y.-Q., et al. 2012, RAA, 12, 1197
Cutri, R. M., Skrutskie, M. F., van Dyk, S., et al. 2003, yCat, 2246, 0
Dachs, J., & Wamsteker, W. 1982, A&A, 107, 240
de Grijs, R., Gilmore, G. F., Johnson, R. A., & Mackey, A. D. 2002, MNRAS, 331, 245
del Rio, G., & Huestamendia, G. 1988, A&AS, 73, 425
de Oliveira, M. R., Fausti, A., Bica, E., & Dottori, H. 2002, A&A, 390, 103
Dias, W. S., Alessi, B. S., Moitinho, A., & Lépine, J. R. D. 2002, A&A, 389, 871
Dias, W. S., Monteiro, H., Caetano, T. C., et al. 2014, A&A, 564, A79
Dougherty, S. M., Taylor, A. R., & Clark, T. A. 1991, AJ, 102, 1753
Drew, J. E., Greimel, R., Irwin, M. J., et al. 2005, MNRAS, 362, 753
Fabregat, J., & Torrejón, J. M. 2000, A&A, 357, 451
Fang, X.-S., Gu, S.-H., Hui, H.-K., et al. 2012, RAA, 12, 93
Frolov, V. N., Jilinski, E. G., Ananjevskaja, J. K., et al. 2002, A&A, 396, 125
Gimenez, A., & Garcia-Pelayo, J. 1980, A&AS, 41, 9
Girardi, L., Bertelli, G., Bressan, A., et al. 2002, A&A, 391, 195
Glushkova, E. V., Koposov, S. E., Zolotukhin, I. Y., et al. 2010, AstL, 36, 75
Glushkova, E. V., Zabolotskikh, M. V., Rastorguev, A. S., Grudskaya, A. V., & Koposov, S. E. 2015, BaltA, 24, 360
González, G., & González, G. 1954, BOTT, 1, 3
Gozha, M. L., Koval', V. V., & Marsakov, V. A. 2012, AstL, 38, 519
Haubois, X., Carciofi, A. C., Rivinius, T., Okazaki, A. T., & Bjorkman, J. E. 2012, ApJ, 756, 156
Hsia, C.-H., & Zhang, Y. 2014, A&A, 563, A63
Hubert, A. M., & Floquet, M. 1998, A&A, 335, 565
Hubert, A. M., Floquet, M., Hao, J. X., et al. 1997, A&A, 324, 929
Jaschek, M., Slettebak, A., & Jaschek, C. 1981, Be star terminology., Be Star Newsletter, 4, 9
Keller, S. C., Grebel, E. K., Miller, G. J., & Yoss, K. M. 2001, AJ, 122, 248
Kharchenko, N. V., Piskunov, A. E., Schilbach, E., Röser, S., & Scholz, R.-D. 2012, A&A, 543, A156
Kharchenko, N. V., Piskunov, A. E., Schilbach, E., Röser, S., & Scholz, R.-D. 2013, A&A, 558, A53
Klement, R., Carciofi, A. C., Rivinius, T., et al. 2015, A&A, 584, A85
Kourniotis, M., Bonanos, A. Z., Soszyński, I., et al. 2014, A&A, 562, A125
Kraus, S., Monnier, J. D., Che, X., et al. 2012, ApJ, 744, 19
Kronberger, M., Teutsch, P., Alessi, B., et al. 2006, A&A, 447, 921
Kubát, J., Korčáková, D., Kawka, A., et al. 2007, A&A, 472, 163
Kulkarni, S. R. 2013, ATel, 4807, 1
Kulkarni, S. R. 2016, in AAS Meeting 227 Abstracts, 314.01
Labadie-Bartz, J., Pepper, J., McSwain, M. V., et al. 2017, AJ, 153, 252
Laher, R. R., Surace, J., Grillmair, C. J., et al. 2014, PASP, 126, 674
Law, N. M., Kulkarni, S. R., Dekany, R. G., et al. 2009, PASP, 121, 1395
Lee, C.-D., & Chen, W.-P. 2011, in IAU Symp. 272, Active OB Stars: Structure, Evolution, Mass Loss, and Critical Limits, ed. C. Neiner et al. (Cambridge: Cambridge Univ. Press), 366
Lee, C.-D., Liu, S.-Y., & Chen, W.-P. 2016, in ASP Conf. Ser. 506, Bright Emissaries: Be Stars as Messengers of Star-Disk Physics, ed. T. A. A. Sigut & C. E. Jones (San Francisco, CA: ASP), 111
Lee, S. H., & Lee, S.-W. 1996, PKAS, 11, 139
Lee, U., Osaki, Y., & Saio, H. 1991, MNRAS, 250, 432
Leisawitz, D., Bash, F. N., & Thaddeus, P. 1989, ApJS, 70, 731
Lin, C.-C., Hou, J.-L., Chen, L., et al. 2015, RAA, 15, 1325
Littlefair, S. P., Naylor, T., Jeffries, R. D., Devey, C. R., & Vine, S. 2003, MNRAS, 345, 1205
Majewski, S. R., Schiavon, R. P., Frinchaboy, P. M., et al. 2015, arXiv:1509.05420
Marsh Boyer, A. N., McSwain, M. V., Aragona, C., & Ou-Yang, B. 2012, AJ, 144, 158
Martayan, C., Baade, D., & Fabregat, J. 2009, in IAU Symp. 256, The Magellanic System: Stars, Gas, and Galaxies, ed. J. T. Van Loon & J. M. Oliveira (Cambridge: Cambridge Univ. Press), 349
Mathew, B., & Subramaniam, A. 2011, BASI, 39, 517
Mathew, B., Subramaniam, A., & Bhatt, B. C. 2008, MNRAS, 388, 1879
McNally, D. 1965, Obs, 85, 166
McSwain, M. V., & Gies, D. R. 2005, ApJS, 161, 118
McSwain, M. V., Huang, W., & Gies, D. R. 2009, ApJ, 700, 1216
Mennickent, R. E., Pietrzyński, G., Gieren, W., & Szewczyk, O. 2002, A&A, 393, 887
Mermilliod, J. C., Mayor, M., & Udry, S. 2008, A&A, 485, 303
Merrill, P. W., Humason, M. L., & Burwell, C. G. 1925, ApJ, 61, 389
Moffat, A. F. J., & Vogt, N. 1975, A&AS, 20, 85
Morgan, W. W., Code, A. D., & Whitford, A. E. 1955, ApJS, 2, 41
Okazaki, A. T. 1997, A&A, 318, 548
Ortolani, S., Carraro, G., Covino, S., Bica, E., & Barbuy, B. 2002, A&A, 391, 179
Pan, Y., Luo, Z.-Q., Zhang, X.-B., et al. 2016, RAA, 16, 109
Pápics, P. I., Tkachenko, A., Van Reeth, T., et al. 2017, A&A, 598, A74
Paul, K. T., Subramaniam, A., Mathew, B., & Shruthi, S. B. 2017, NewA, 56, 28
Paunzen, E., Schnell, A., & Maitzen, H. M. 2005, A&A, 444, 941
Pecaut, M. J., & Mamajek, E. E. 2013, ApJS, 208, 9
Pecaut, M. J., Mamajek, E. E., & Bubar, E. J. 2012, ApJ, 746, 154
Percy, J. R., Hosick, J., Kincaide, H., & Pang, C. 2002, PASP, 114, 551
Piskunov, A. E., Schilbach, E., Kharchenko, N. V., Röser, S., & Scholz, R.-D. 2008, A&A, 477, 165
Pojmanski, G. 1997, AcA, 47, 467
Pojmański, G. 2001, in ASP Conf. Ser. 246, IAU Coll. 183: Small Telescope Astronomy on Global Scales, ed. B. Paczynski, W.-P. Chen, & C. Lemme (San Francisco, CA: ASP), 53
Porter, J. M., & Rivinius, T. 2003, PASP, 115, 1153
Raboud, D., & Mermilliod, J.-C. 1998, A&A, 333, 897
Raddi, R., Drew, J. E., Steeghs, D., et al. 2015, MNRAS, 446, 274
Ren, A., Fu, J., De Cat, P., et al. 2016, ApJS, 225, 28
Rieke, G. H., & Lebofsky, M. J. 1985, ApJ, 288, 618
Rivinius, T., Baade, D., & Carciofi, A. C. 2016, A&A, 593, A106
Rivinius, T., Baade, D., & Štefl, S. 2003, A&A, 411, 229
Rivinius, T., Carciofi, A. C., & Martayan, C. 2013, A&ARv, 21, 69
Roeser, S., Demleitner, M., & Schilbach, E. 2010, AJ, 139, 2440
Sabogal, B. E., García-Varela, A., & Mennickent, R. E. 2014, PASP, 126, 219
Saio, H., Ekström, S., Mowlavi, N., et al. 2017, MNRAS, 467, 3864
Salaris, M., Weiss, A., & Percival, S. M. 2004, A&A, 414, 163
Saurin, T. A., Bica, E., & Bonatto, C. 2015, MNRAS, 448, 1687
Schild, R., & Romanishin, W. 1976, ApJ, 204, 493
Souza, S. P., Garcia Soto, A., & Wong, H. 2016, in AAS Meeting 228 Abstracts, 319.03
Subramaniam, A., Gorti, U., Sagar, R., & Bhatt, H. C. 1995, A&A, 302, 86

Tarasov, A. E., & Malchenko, S. L. 2012, AstL, 38, 428
Townsend, R. H. D., Owocki, S. P., & Howarth, I. D. 2004, MNRAS, 350, 189
van Cauteren, P., Lampens, P., Robertson, C. W., & Strigachev, A. 2005, CoAst, 146, 21
Wang, J., Townsley, L. K., Feigelson, E. D., et al. 2008, ApJ, 675, 464
Wisniewski, J. P., & Bjorkman, K. S. 2006, ApJ, 652, 458
Wisniewski, J. P., Bjorkman, K. S., Magalhães, A. M., et al. 2007, ApJ, 671, 2040
Woolf, N. J., Stein, W. A., & Strittmatter, P. A. 1970, A&A, 9, 252
Wright, E. L., Eisenhardt, P. R. M., Mainzer, A. K., et al. 2010, AJ, 140, 1868
Yu, P. C., Lin, C. C., Chen, W. P., et al. 2015, AJ, 149, 43
Yu, P.-C., Lin, C.-C., Lin, H.-W., et al. 2016, AJ, 151, 121
Zhang, C., Fu, J. N., & Jiang, X. J. 2008, JPhCS, 118, 012078
Zhang, P., Chen, P. S., & Yang, H. T. 2005, NewA, 10, 325